Doped Oxides for High-Temperature Luminescence and Lifetime Thermometry

M.D. Chambers[1] and D.R. Clarke[2]

[1]Materials Department, College of Engineering, University of California, Santa Barbara, California 91360-5050; email: chambers@engineering.ucsb.edu

[2]School of Engineering and Applied Sciences, Harvard University, Cambridge, Massachusetts 02138

Annu. Rev. Mater. Res. 2009. 39:325–59

The *Annual Review of Materials Research* is online at matsci.annualreviews.org

This article's doi:
10.1146/annurev-matsci-112408-125237

1531-7331/09/0804-0325$20.00

Key Words

thermal barrier coating, environmental barrier coating, rare earths, decay, zirconia, silicates

Abstract

The measurement of high temperatures in oxides and oxide-based structures in practical applications often presents challenges including steep thermal gradients, the presence of flames or chemically aggressive environments, and the transparency or translucency of most oxides. For turbine engines, oxide coatings are of great commercial importance, and the rapid motion of parts prohibits contact thermometry. Luminescence thermometry offers a number of advantages for measuring temperature in such systems and has been the subject of ongoing study for many years. Recent work on rare-earth-doped thermal barrier coatings, environmental barrier coatings, and related oxides has demonstrated the feasibility of luminescence thermometry to temperatures well in excess of 1000°C. The luminescent properties of these materials and the analytical techniques used to extract reproducible temperature measurements from the measured luminescence are reviewed.

1. INTRODUCTION

One of the challenges in using oxides at high temperatures, especially in some of the newer structural applications, is to measure their temperature, particularly at and below the surface and under transient conditions. For instance, oxides are increasingly being used as thermal barrier coatings (TBCs) in high-temperature gas turbines to provide thermal protection to both stationary and rotating components so as to enable turbines to operate at higher temperatures and energy efficiencies. In this important application, the coatings are subject to large thermal gradients, and the maximum temperature of the metal components beneath the coating should not exceed a given design temperature during service; otherwise the lifetime of the component is severely compromised. The inaccessibility and motion of the components make contact thermometry difficult or impossible. Similarly, the translucent nature of most oxides poses problems for pyrometry (aside from the well-known uncertainty in emissivity) when the oxide is under a temperature gradient because the thermal radiation sampled by the pyrometer originates from material at different depths and temperatures. A comparison of pyrometry and luminescence thermometry (and other techniques) is reviewed elsewhere (1).

An alternative method of measuring temperature is by luminescence thermometry: the determination of temperature from characteristic, temperature-dependent aspects of the luminescence, such as spectral features, intensity, and lifetime. This was first demonstrated in the 1950s by use of phosphors painted onto an aircraft wing section in a wind tunnel to measure aerodynamic heating (2) and has been used in a variety of measurement applications since. A decade ago, Allison & Gillies (3) reviewed the status of the field and various measurement techniques. The focus of much of the work in the field at that time was on the development of suitable phosphors for thermometric paints (3) and materials coupled to fiber optics to create optical temperature probes analogous to thermocouples (4).

As distinct to the development of thermometric paints in which the phosphor serves the single purpose of temperature measurement, recent work has been directed toward adding thermometric functionality, by doping with luminescent activators, to materials already selected for particular applications on the basis of their other properties. Such a doped oxide can function as a sensor intrinsic to a system in which the oxide is normally used anyway or as an extrinsic sensor in another system wherein the oxide would not ordinarily be present. In this review, we describe recent developments in characterizing appropriate dopants, or activators, for several oxides that are used in high-temperature applications, such as the TBC mentioned above, as well as the demonstration of these materials as sensor layers. We also describe recent advances in the analysis and precision of temperature measurement by luminescence thermometry.

One of the goals of research in this field has been to push the limit of temperature measurement capability to higher temperatures. For this reason we focus on dopants with long-lived excited states at temperatures above 800°C and on refractory oxide hosts capable of withstanding sustained exposure to high temperatures. We also describe progress in the understanding of decay phenomena that may result in not only better predictions of what dopant-host combinations may lead to high-temperature sensitivity but also increased precision through decay analysis and materials engineering.

2. ESSENTIALS OF LUMINESCENCE LIFETIME THERMOMETRY

A simplified luminescent system is depicted in **Figure 1*a***, which shows the energy levels of a dopant in a host. An incident light pulse excites some portion of the dopant population from the ground state (level 0) to its excited state (level 1), after which ions in the excited state decay probabilistically back to the ground state either by reemitting the absorbed energy as a photon

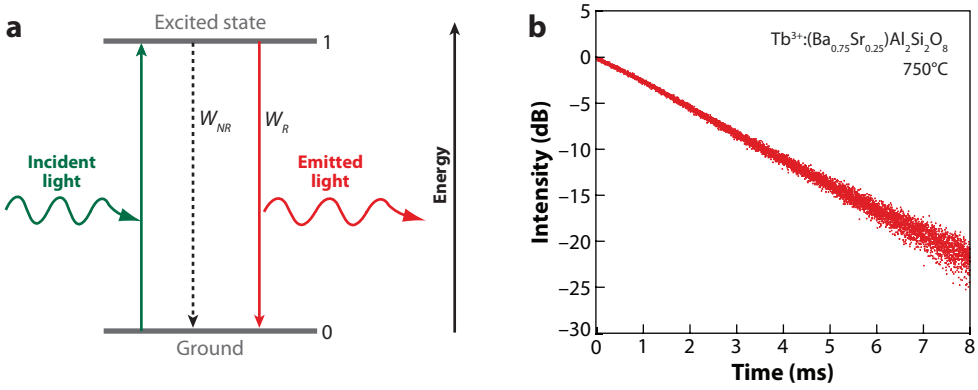

Figure 1

(*a*) Schematic diagram showing a simplified, two-level system. Deexcitation occurs by competing radiative and nonradiative processes. (*b*) An example of a luminescence decay from $Tb:(Ba_{0.75}Sr_{0.25})Al_2Si_2O_8$ that is representative of the exponential decay from such a two-level system.

or by dissipating that energy as heat. These processes have different probabilities of occurring (considering a single excited ion), or different rates (considering the whole population of excited ions), and are competitive with one another. The emission (and absorption) spectrum of this simple system is a single peak corresponding to the energy difference between levels 1 and 0. The lifetime, τ, of the emission is determined by the rates, W, of all decay processes, both radiative and nonradiative:

$$\frac{dN_1}{N_1} = -\left(W_{1\to0}^{Radiative} + W_{1\to0}^{Nonradiative}\right)\cdot dt, \qquad 1.$$

the solution of which leads to an exponential decay expression:

$$N_1(t) = N_1^0 \exp\left(\frac{-t}{\tau}\right) \qquad 2a.$$

or, equivalently, in terms of emission intensity:

$$I(t) = I_0 \exp\left(\frac{-t}{\tau}\right), \qquad 2b.$$

where the lifetime τ is

$$\tau \equiv \left(\sum_i W_i\right)^{-1}, \qquad 3.$$

which is the slope of the decay as seen in **Figure 1*b***.

Luminescence can be used as a measure of temperature through the temperature dependence of any aspect of these processes. For instance, the frequency of the emission peak depends on the temperature-dependent position of the energy levels. Similarly, the lifetime of the emitting level is determined by W_R and W_{NR}, both of which may be temperature dependent (although W_{NR} is usually much more so). The intensity of the peak also depends on the rates of the competing decay processes because the intensity I, or number of emitted photons, equals the number of ions that decay by the process $W_{1\to0}^R$:

$$I_{1\to0}(t) = N_1(t)\cdot W_{1\to0}^{Radiative} \Rightarrow I_{1\to0}^{total} = \int_0^\infty N_1(t)\cdot W_{1\to0}^{Radiative}\cdot dt. \qquad 4a,b.$$

All these properties of a material's luminescence have been used to measure temperature (3), but the lifetime has a number of advantages over the spectral features (the wavelength and intensity of the emissions), especially at high temperatures. First, spectra can be convoluted by black-body radiation, flame emissions and absorptions, and contamination of the emitting material. These convolutions can be considerable for many systems for which luminescence thermometry has been investigated, such as jet turbine engines (5) and combustion surfaces (6). (Other spectral techniques of thermometry, such as Raman scattering and pyrometry, are also affected by these artifacts.) In contrast, these do not affect lifetime data except in that they decrease the signal-to-noise ratio and can, with very bright black-body radiation, lead to detector saturation artifacts. Additionally, the precision to which time can be resolved with commercial instruments is very much greater than the precision to which spectra can be resolved (see Reference 1 for a comparison), and the loss of intensity ubiquitously experienced at high temperatures is much more pronounced in the spectrum than in the decay trace of intensity (see Section 9.2).

In practice Equation 2 is too simple to accurately describe most observed luminescence. Most activators have numerous energy levels—**Figure 2** shows, for instance, the energy levels of the 13 optically active rare earths that vary little with crystal field. Even Yb^{3+} shows sufficient Stark splitting of its upper and lower level in most hosts to preclude description by Equation 2.

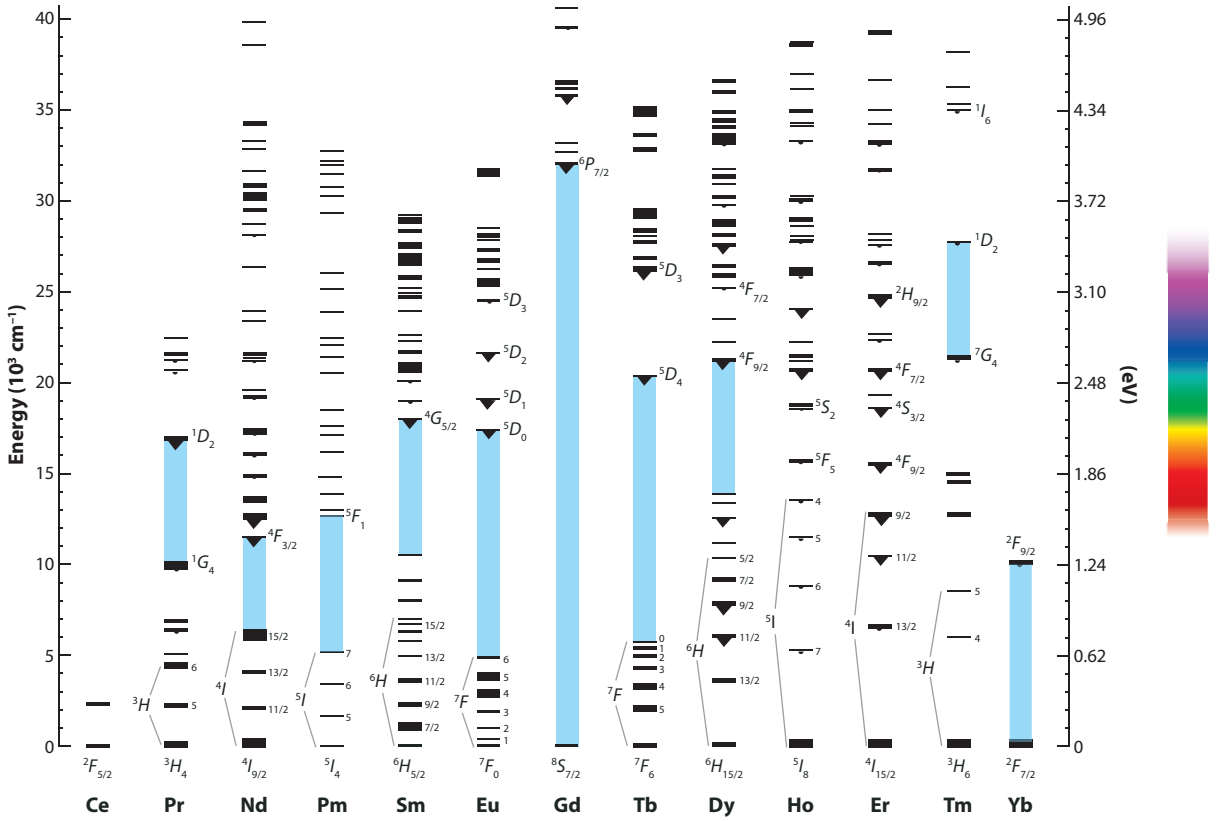

Figure 2

The Dieke energy diagram for the trivalent rare earths from Ce^{3+} to Yb^{3+}. Drawn after Reference 120, with slight modifications based on References 121 and 122. The blue shading between levels marks the largest energy gap for the rare earths shown.

To describe the simplest real systems, the populations of multiple excited levels, multiple radiative and nonradiative transitions from each level, and the contribution to W_{NR} of processes other than direct relaxation (described in Section 8) must also be considered. That is, ignoring the distinction between different processes contributing to each $W_{i\to j}$,

$$|dN_i|_i = -|W_{ij}^{-}(T)|_{ij}|N_j|_j \cdot dt, \qquad 5.$$

where diagonal elements indicate total decay rates and off-diagonal elements are negative and indicate the filling of one level from another.

In many oxides the luminescent ions may also occupy more than one kind of crystallographic site. Each population of ions in a particular kind of site may show different spectral and decay features, and the excited-state populations of each population must be considered separately. Additionally, many dopant ions can interact with each other or with impurities if they are close enough. This leads to a further subset of populations based on nearest-like-neighbor distances. In the most complex cases, interplay between the different site populations must also be considered.

3. DOPANT SELECTION

Rare-earth ions, or lanthanides (i.e., Ln^{3+}), transition metals, and heavy metals are optically active, capable of absorption and emission in the visible spectrum. There are four criteria for selecting an activator to achieve high-temperature thermometry with a given host material:

- strong emission, preferably toward the blue region of the visible spectrum,
- solubility in the host with the desired oxidation state,
- no adverse effects on the host's other properties, and
- simultaneous minimization of all nonradiative processes.

The first criterion is motivated by signal strength considerations. Short-wavelength emissions are preferable to longer-wavelength emissions because at high temperatures the background from black-body radiation is considerable and depends inversely on wavelength to the fourth power (that is, the number of photons emitted, not the power) (see **Figure 3**). Emissions with too short

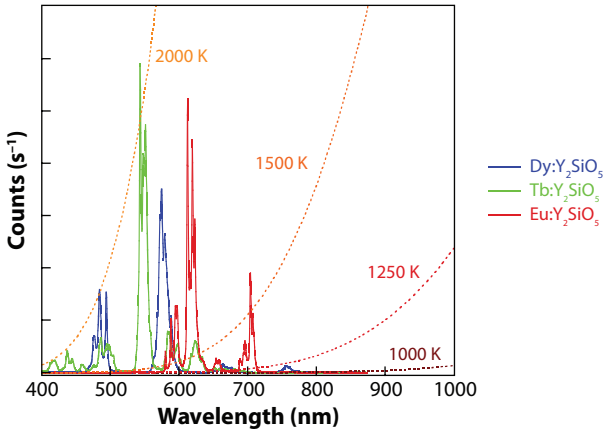

Figure 3

Characteristic emission spectra for three different rare earths in Y_2SiO_5 plotted together with the black-body spectra for the indicated temperatures. At high temperatures the black-body radiation is a background signal above which the emission spectra have to be detected, limiting the attainable signal-to-noise ratio for thermometry.

a wavelength, into the UV, can be difficult to collect and accurately measure, and in the extreme case the emission may be past the host's absorption edge, which prevents any signal from escaping.

The second criterion is simply that the activator must go into the host's crystal lattice and remain in its optically useful ionization state. Most rare earths possess the advantage of very strongly preferring the trivalent state regardless of their host (although Sm, Eu, and Yb, in order of propensity, can become divalent, and Ce and Tb can become tetravalent). Furthermore, most rare earths can readily be accommodated as trivalent ions in small to large concentrations in numerous high-temperature oxides, including perovskites, silicates, and zirconates.

Satisfaction of the fourth criterion is the most difficult to predict a priori because there are a variety of ways by which an activator may decay nonradiatively, including direct relaxation from one level to another; thermal promotion from the emitting level to a higher-energy, shorter-lived level; and cross-relaxation between ions. All these processes are temperature dependent, and in practice the most competitive of them determines the temperature sensitivity of the excited-state lifetime. Direct relaxation by multiple phonon emission, or multiphonon relaxation (MPR), is controlled largely by the energy gap between the excited state and the level to which the excited state relaxes (usually only the next lower level is considered) and by the amount of energy that must be dissipated. Decay by promotion to a shorter-lived level depends on the existence and position of such a level, especially charge-transfer states (CTS) for the rare earths and the $^4T_2$ level in $3d^3$ transition metal ions. Cross-relaxation depends on the energy matching of upward transitions with downward transitions. Moreover, the electrons responsible for the optical activity of the Ln^{3+} ions show less sensitivity to thermal effects such as lattice vibrations and crystal field distortions, which, for other ions, can broaden energy levels and contribute to nonradiative decay (as in Reference 7). Section 8 considers these matters further.

4. LUMINESCENCE OF ZIRCONIA-BASED MATERIALS

4.1. Doped Stabilized Zirconia

Yttria-stabilized zirconia (YSZ) is the current material of choice for TBCs in gas turbine engines. With a composition of $Y_{0.076}Zr_{0.924}O_{1.962}$, this oxide has unusually low, and temperature-independent, thermal conductivity. This is attributed to the high concentration of oxygen vacancies introduced to charge-compensate the Y^{3+} ions, which also stabilize the tetragonal phase. From a thermal conductivity perspective, it has a glassy structure, and for this reason it had been argued that the luminescence would be weak and would extend to only moderate temperatures.

Nevertheless, YSZ doped with a variety of rare earths, including Eu^{3+}, Sm^{3+}, Dy^{3+}, Tm^{3+}, and Er^{3+} (but not Tb, which tends to form Tb^{4+}), exhibits strong luminescence to high temperatures and has thermal sensitivity up to at least 1100°C (8–10). **Figure 4** shows a series of calibration curves relating lifetime to temperature for some of the longest-lived activators along with a figure of merit for the temperature sensitivity, the ratio of uncertainty between the measured lifetime and the derived value for temperature (see Section 9.2 for a discussion). Ho^{3+} in YSZ is reported to luminesce brightly at 549 nm (11), but there are no reports of its lifetime. Cr^{3+}:YSZ does not luminesce brightly, even at room temperature in YSZ, in which the short-lived $^4T_{2g}$ state is thought to lie beneath that of the ^2E_g state (12). Of the dopants indicated in **Figure 4**, Eu^{3+} and Sm^{3+} show strong CTS in their excitation spectra and the high temperature decay of Eu^{3+} is thought to be primarily through the CTS since direct relaxation to $^7F_6$ is expected to be sluggish due to the large gap. For Sm^{3+} the possibility of cross-relaxation also exists. Dy^{3+} shows only a weak CTS in YSZ but shows strong cross-relaxation and self-quenching, and we have observed decreases in intensity and in both room-temperature and high-temperature lifetimes with concentration. Indeed, at a

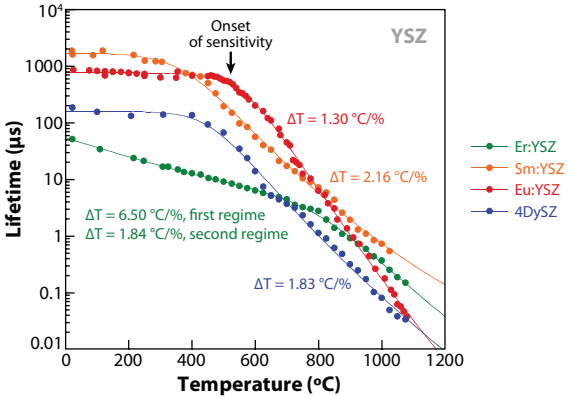

Figure 4

Fitted lifetime-versus-temperature curves for Er, Eu, Dy, and Sm in yttria-stabilized zirconia (YSZ).

concentration of 12% Dy ($Dy_{0.12}Zr_{0.90}O_{1.94}$), all luminescence is quenched. Er^{3+} ($^4S_{3/2}$) shows a lifetime-temperature curve with two regimes of temperature dependence. Merino et al. (13) report a satisfactory fit using a MPR model that accounts for thermalization from $^4S_{3/2}$ to higher levels; we have fit the data satisfactorily using a combination of MPR from $^4S_{3/2}$ and thermal promotion to the fast-emitting $^2H_{11/2}$ level.

The origin of the bright luminescence from the rare earths is attributed to the local deviations from the almost cubic symmetry of the crystal structure introduced by local field distortions due to the statistical replacement of Zr^{4+} with Y^{3+} and Ln^{3+}, and of O^{2-} with vacancies, distortions that relax the selection rules governing radiative transitions. The distortions also result in populations of activator ions with different local symmetries and potentially different lifetimes and quenching behavior. Indeed, a feature of the luminescence decays from the various rare-earth doped YSZ is that they are rarely single-exponential in character and must be fit with more complex functions. Their decay character depends on processing conditions (YSZ is normally metastable) and can also vary with temperature. For instance, for 1% Eu-doped YSZ (i.e., $Eu_{0.01}Y_{0.07}Zr_{.092}O_{1.96}$) the luminescence decay usually consists of two exponential components, a fast decay and a slow decay. The slower one was used in constructing **Figure 4**.

The local coordination of Y^{3+} and Ln^{3+} in YSZ is not completely known. For instance, EXAFS studies indicate that Y^{3+} and Gd^{3+} ions have a coordination of 8 and the oxygen vacancies have a preference to be next-nearest neighbors to the dopant ion (14). However, site-selective spectroscopy studies have found that Eu^{3+} in stabilized cubic zirconias occupies at least two major site types (15, 16). Merino has deduced from the fine structure of the luminescence spectra that there are populations of Dy^{3+} having sixfold, sevenfold, and eightfold coordinate in YSZ (which he attributes to the association of 2, 1, or 0 vacancies respectively) (17) and at least sevenfold and eightfold coordination for Er^{3+} in YSZ (13). On the other hand, Nd^{3+} has been reported to occupy a single site type (18), presumably due to a stronger site preference associated with its larger ionic radius.

To gain a more complete picture, systematic studies on the effect of stabilizer concentration, activator concentration, and thermal aging of stabilized zirconia, with and without Y^{3+}, have been performed using the luminescence from the Eu^{3+} as a probe since it does not show strong self-interactions [it is luminescent in even very high concentrations (10, 19)]. It was found that the strengths of the various emissive transitions, as seen in the emission spectra, change with phase evolution, and thus, necessarily, the overall radiative decay rate changes with prolonged, high temperature aging. Room-temperature lifetimes can range from 200 μs to 2 ms, and the decay character can

be either single exponential or strongly double-exponential, indicative of two significantly different Eu^{3+} populations. The decays also show an increase in double-exponential character near and above the onset of temperature sensitivity. Above that onset the longest lifetimes of tetragonal and cubic Eu-doped zirconias, with different stabilizer concentrations and thermal histories, converge. The reason for this is thought to be that, while room-temperature lifetimes depend on the radiative transition strengths, the operative nonradiative processes are insensitive to the radiative rate as well as the small changes in site symmetry that affect the emission spectra. The presence of fast and slow components of the decay at high temperatures is ascribed to the presence of different Eu^{3+} populations for which W_{NR} is determined differently—for instance, if a CT decay pathway is governing W_{NR} (8, 20) then the difference in the energy of that state for 7-coordinate and 8-coordinate sites (the two most populous kinds) could account for the double-exponential decay character.

The types of crystallographic site populations present in 7YSZ also depend on the processing and thermal history of the material because homogeneous 7YSZ, which has a tetragonal crystal structure referred to as t', phase-separates at high temperatures into low- and high-stabilizer content phases. Subsequently, the former may transform to a monoclinic crystal structure. This results in a variety of subpopulations within the six-, seven-, or eight-coordinate sites depending on the local stabilizer content and crystal structure. Thus, the decay behavior from Ln^{3+}:7YSZ is often convolved with rich information about the thermal age and in many cases is only approximately singly or doubly exponential. Furthermore, some ions that can undergo cross-relaxation, such as Sm^{3+}, Er^{3+}, and Dy^{3+}, usually show nonexponential decays due to strong self-interaction at even 1% concentration. This is because, for these ions, each population of ions is further divided depending on the distance from one dopant ion to the next-nearest dopant ion (see discussion on cross-relaxation in Section 7.4, below), each with a slightly different decay rate. However, despite these complications the temperature dependence of the luminescence lifetime of the Ln^{3+}-doped 7YSZ materials are characteristic of the rare-earth dopant used and highly reproducible for a given dopant and concentration.

The unusual behavior of Er^{3+} may be attributed to the involvement of the $^2H_{11/2}$ level, which lies immediately above the primary emitting level, $^4S_{3/2}$ (21), and serves as a low-activation energy alternative decay pathway. The downward transitions from $^2H_{11/2}$ are stronger than those from $^4S_{3/2}$ (22–24). Thus, as thermal excitation from $^4S_{3/2} \rightarrow {}^2H_{11/2}$ increases with temperature, the lifetime of $^4S_{3/2}$ decreases. This forms the first part of the calibration curve, which slopes fairly gently until a stronger process (possibly direct relaxation) overtakes it at approximately 750°C. [See the thermalization equation (Equation 8) in Section 8.]

Finally, as zirconia materials—such as those used in fuel cell electrolytes, oxygen sensors, and turbine combustor liners—are used in a wide variety of atmospheres, detailed investigation of the effects of oxygen stoichiometry has begun. Studies have found that vacancies in 7YSZ produced by annealing in reducing atmospheres, down to pO_2 of 10^{-11} ppm, have no discernable effect on the lifetime behavior of Dy^{3+} and Eu^{3+} (**Figure 5** and Reference 25), although the partial reduction does decrease the overall luminescence intensity. Furthermore, the lifetimes are unaffected by repeated cycling between oxidizing and reducing anneals. This insensitivity is attributed to the fact that the number of oxygen vacancies produced under even highly reducing atmospheres is greatly outnumbered by the number of vacancies required to charge balance the Y^{3+} stabilizer concentration.

4.2. Rare-Earth Zirconates

Another class of materials used as TBCs are the rare-earth zirconates, $Ln_2Zr_2O_7$ (26, 27) for Ln^{3+} between La^{3+} and Gd^{3+}. These materials have lower thermal conductivity than does YSZ

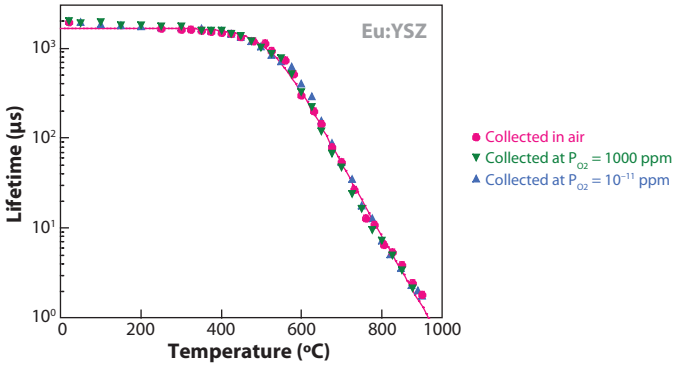

Figure 5

The effect of atmosphere, air, and reducing atmosphere on the luminescence lifetimes recorded in situ for Eu:7YSZ. As illustrated, the effect of measurement in even extremely low-oxygen atmospheres is negligible. After Reference 123.

(28) and have increased chemical stability against sand ingested in jet turbine engines (29, 30). In the zirconates, rare-earth activators substitute for a chemically similar stabilizer ion in a cubic (pyrochlore) crystal but have noncubic local symmetry due to the numerous vacancies and the statistical distribution of Ln^{3+} and Zr^{4+} ions. The use of Tb is again precluded due to the formation of Tb^{4+} rather than of Tb^{3+} (31).

Gentleman & Clarke (10) made an in-depth study of Eu^{3+}-doped zirconate materials, including $Gd_2Zr_2O_7$, $Sm_2Zr_2O_7$, and $Eu_2Zr_2O_7$. Eu:$Gd_2Zr_2O_7$ showed lifetimes similar to that of Eu:YSZ, including a strong double-exponential character. Eu:$Sm_2Zr_2O_7$ showed decreased high-temperature lifetimes and, thus, a lower maximum temperature of sensitivity, but notably the lifetime-temperature curve for Eu:$Sm_2Zr_2O_7$ matched the fast lifetimes of Eu:$Gd_2Zr_2O_7$. Because Sm^{3+} can interact with Eu^{3+} through its $^5G_{5/2}$ level (32) (which is only slightly higher in energy than the $^5D_0$ level of Eu^{3+}), there are two possible explanations for the observed behavior. First, the population of activators responsible for the long lifetime is being preferentially quenched by interaction with the surrounding Sm^{3+} (which, in such high concentration, effectively self-quenches by cross-relaxation and dissipation to quenching sites). Second, the luminescent intensity of Eu^{3+} is being diminished uniformly by its host, and the long lifetime could not be resolved above the noise.

One unexpected finding is that Eu^{3+} remains luminescent at very high concentrations in $Gd_2Zr_2O_7$, even up to the complete substitution of Eu^{3+} for Gd^{3+}, that is, $Eu_2Zr_2O_7$. Also unexpected is that Gentleman & Clarke found a monotonic increase in the high-temperature lifetimes going across the series $(Gd_{1-x}Eu_x)_2Zr_2O_7$, albeit with a decrease in intensity after approximately 20% Eu [see Reference 33; see also Reference 10 for end-member compositions]. The origin of the increase in lifetime remains to be elucidated.

5. LUMINESCENCE OF SILICATES

5.1. Rare-Earth Silicates

Many designs for future turbines are based on the replacement of metallic alloys in the highest-temperature areas of the engine by ceramic components, principally SiC because of its combination of thermal shock resistance and high-temperature strength. However, because SiC is prone

to volatilization at high temperature when exposed to high-velocity air containing moisture, it is generally accepted that the components will have to be coated with an environmental barrier coating (EBC) to protect the SiC (34, 35). Rare-earth silicates of the form Ln_2SiO_5 and $Ln_2Si_2O_7$ have shown considerable promise in this application, and those based on yttrium have been shown special interest. As with the zirconia-based oxides, these silicates can be doped with small concentrations of rare-earth ion to become luminescent. The rare-earth ions substitute for Y^{3+} because of the similarity in ionic radii (36, 37), but unlike in YSZ, they occupy inherently low-symmetry sites in these materials [C_1 and C_2 sites for the $X2$ phase of Y_2SiO_5, C_1 and C_i for D-type $Y_2Si_2O_7$ (38–40)]. Thus, they show very bright luminescence at room temperatures (41).

High-temperature lifetime studies of Eu:Y_2SiO_5 ($X2$) and Eu:$Y_2Si_2O_7$ (type D) have shown strong luminescence with a temperature sensitivity between approximately 700°C and 1200°C (20). These data are supplemented with additional data for two other rare earths, Tb^{3+} and Dy^{3+}, that we present for the first time here in **Figure 6** (see Reference 20 for experimental details). All the doped silicates show strong luminescence at high temperatures with sensitivity ranging from 700°C to at least 1440°C (the limit of the testing equipment) with a variety of sensitivities; Tb^{3+} shows the strongest temperature dependence (see Section 9.2). All the $Y_2Si_2O_7$ materials, and the Tb:Y_2SiO_5, showed emissions from the next higher level from the main emitting level and rise times in the emissions from the main level. These faster decays could be used to extend the range of sensitivity to lower temperatures.

One of the challenges in implementing luminescence thermometry with functional silicate materials is the frequent presence of metastable phases in silicate coatings. For instance, Y_2SiO_5 forms both a low-temperature $X1$ phase and a high-temperature $X2$ phase (38). $Ln_2Si_2O_7$ can adopt seven different crystal structures, depending on temperature and rare-earth ionic radius, of which four are stable at high temperatures (42, 43). Additionally, several EBC designs involve

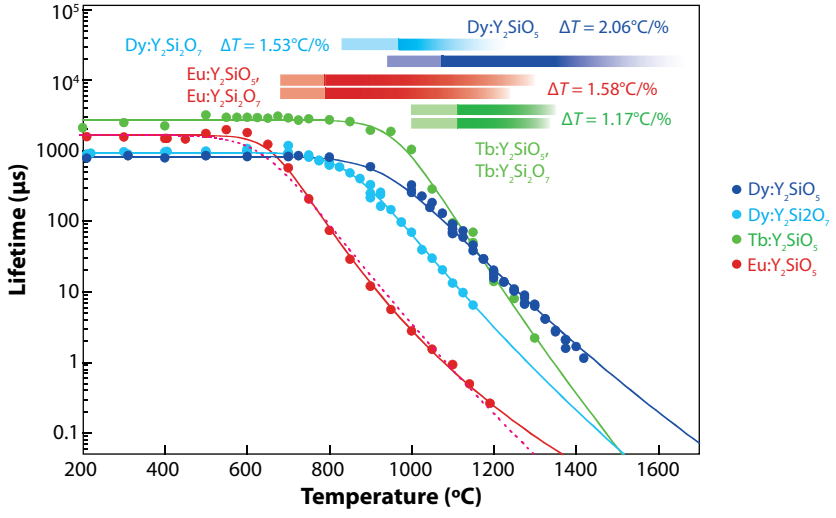

Figure 6

Fitted lifetime-versus-temperature curves for Dy, Eu, and Tb in Y_2SiO_5 and $Y_2Si_2O_7$, candidates for environmental barrier coatings. Eu:Y_2SiO_5 has been fitted with both CTS (*solid*) and MPR (*dashed*) models to demonstrate the better appropriateness of CTS for this kind of curve. Horizontal bars represent the ranges of temperature sensitivity for the different dopants. The lighter sections of the bars correspond to lifetimes that are too long for accurate temperature measurement on a surface rotating at 16,000 RPM (5).

composites consisting of a mixture of phases, e.g., Y_2SiO_5 and $Y_2Si_2O_7$ together (44, 45), and $Y_2Si_2O_7$ also slowly transforms to Y_2SiO_5 as it loses silica upon exposure to hot water vapor. Fortunately, the high-temperature lifetimes of Eu^{3+} and Tb^{3+} are similar in both Y_2SiO_5 and $Y_2Si_2O_7$, and so with these dopants a mixture of the two silicates should not complicate thermometry measurements. In contrast, Dy^{3+} shows a much shorter high-temperature lifetime in the disilicate than in the monosilicate; however, the intensity also quenches much more quickly such that at 900°C the longer-lived monosilicate has an intensity advantage by a factor of ten, which increases further at higher temperatures. This high-temperature dominance may allow a possible mixture of Dy:Y_2SiO_5/Dy:$Y_2Si_2O_7$ to be used for thermometry.

The dissimilarity in room-temperature lifetimes for Eu^{3+} and Tb^{3+} between hosts is due to differences in radiative emission strengths, whereas the similarity of high-temperature lifetimes indicates that the nonradiative process controlling the high temperature decays is similar. For Eu^{3+} a CTS path is likely; the fit lines in **Figure 6** demonstrate that the CTS model is more appropriate to handle the significantly curving high-temperature part of the calibration curve. For Tb^{3+} it is tempting to assign a decay path through $4f^7 5d^1$ because the energy barriers to both direct relaxation and thermalization are very large, cross-relaxation is not possible, and the CTS state is very high (see Section 7; **Table 1**). The process governing the temperature dependence of the lifetimes of Dy^{3+} is less clear. Studies measuring the effect of concentration, possible filling of lower emissive levels (e.g., $^6F_{5/2}$), and the lifetime of potential thermalized levels ($^4I_{15/2}$) will be necessary to determine which of several processes is dominant.

5.2. Other Silicates

Another class of materials that have been investigated for EBC use is the modified celsian compounds such as BSAS [$(Ba_{0.75}Sr_{0.25})Al_2Si_2O_8$]. Rare earths can be doped into BSAS to produce luminescence, with the rare earth presumably substituting on the Ba^{2+}/Sr^{2+} sites (46, 47) considering ionic radii, although solubility is expected to be limited. Divalent rare earths, notably Sm^{2+}, Eu^{2+}, and Yb^{2+}, are easily formed by reducing atmospheres in $BaAl_2Si_2O_8$ (48–50).

Like the rare-earth silicates, BSAS goes through a phase transition at high temperatures, although for EBC applications the lower-temperature conformation, monoclinic celsian, is desired because the high-temperature phase, hexacelsian, possesses a coefficient of thermal expansion that is significantly mismatched with that of SiC-SiC ceramic matrix composites (51). There have been relatively few luminescence studies of monoclinic BSAS. Therefore, we present data on the luminescent lifetime of Eu:BSAS, Tb:BSAS, and Dy:BSAS [that is, $(Ln_{0.01}Ba_{0.74}Sr_{0.25})Al_2Si_2O_8$] as a function of temperature, measured by techniques described elsewhere (52). **Figure 7** shows the lifetime-temperature curves for these materials. Eu^{3+} shows lifetimes comparable to those in YSZ, whereas Tb and Dy show sensitivity up to at least 1200°C. Compared with the yttria-silicates, the onset of temperature sensitivity is at a higher temperature for Tb^{3+} and Dy^{3+} and at lower temperature for Eu^{3+}. Tb:BSAS is notable in that, up to the maximum temperature of the experiment, 1440°C, it has the longest observed lifetimes of which we are aware outside of YAG-based sensor materials (see Section 6.1 below). Above 1440°C, on the basis of the greater temperature sensitivity of Tb:BSAS than of Dy:Y_2SiO_5, the lifetime of Dy:Y_2SiO_5 is expected to be longer.

Additionally, all the decays for Tb:BSAS above approximately 500°C showed distinct rise times at the beginning of each decay, attributed to filling of $^5D_4$ from $^5D_3$, the next higher level. This indirect indicator of the lifetime of the $^5D_3$ population can also be used for temperature measurement and, for similar temperatures, shows a shorter time constant than the $^5D_4$ lifetime—a property that is useful for situations in which collection must occur in a narrow time window, such as a rotating turbine blade.

Table 1 A survey of the properties of rare earths important to lifetime-temperature curves

Ion	$4f^{n-1}5d^1$[a]	CTS[b]	Emitting levels	Direct relaxation[c]	Lifetime at RT[d]	Lower level of emission	Emission (nm)[e]	Cross-relaxation[f]	References
Ce^{3+}	0	High	$5d^1$		Very short	$^2F_{5/2}$, $^2F_{7/2}$	Blue	No	129, 146
Pr^{3+}	12.66	19.68	$^3P_0$	3.63	Moderate	$^3H_4$, $^3F_2$	485, 635	$^1D_2 + {}^3H_6 + h\nu$, $^1G_4 + {}^1G_4 + h\nu$	114, 147–149
			$^1D_2$	6.89	Moderate	$^3H_4$	607	$^1G_4 + {}^3F_4$	114, 150
Nd^{3+}	22.67	18.47	$^4F_{3/2}$	5.13	Moderate	$^4I_{11/2}$	1064	$^4F_{3/2} + {}^4I_{15/2} + h\nu$	125
Pm^{3+}	~26.65		$^5F_1$	7.5	Long	$^5I_4$	847	No	151
Sm^{3+}	26.55	9.36	$^4G_{5/2}$	7.47	Long	$^6H_{5/2}$, $^6H_{9/2}$	580, 670	$^6F_{9/2} + {}^6F_{9/2}$	152, 153
Sm^{2+}	<0	High	$^5D_0$	10.46	Long	$^7F_0$, $^7F_2$	690, 730	No	143
Eu^{3+}	35.95	0	$^5D_0$	12.49	Long	$^7F_1$, $^7F_2$	590, 606	No	3, 10, 154
			$^5D_1$	1.68	Short	$^7F_2$	550	$^5D_0 + {}^7F_3$	3, 90
Eu^{2+}	<0	High	$5d^1$		Short	$^8S_{7/2}$	Blue-green	No	155, 156
Gd^{3+}	45.96	High	$^6P_{7/2}$	32.08	Long	$^8S_{7/2}$	311	No	113, 157
Tb^{3+}	4.84 (sf)	High	$^5D_4$	14.63	Long	$^7F_5$	544	No	31, 124
			$^5D_3$	5.82	Moderate	$^7F_5$	438	$^5D_4 + {}^7F_0$	153, this work
Dy^{3+}	17.53 (sf)	16.45	$^4F_{9/2}$	7.41	Long	$^7H_{15/2}$, $^6H_{13/2}$	484, 571	$^6F_{3/2} + {}^6F_{11/2}$, $^6H_{5/2} + {}^6H_{5/2} + h\nu$	126, 157, 158
			$^4F_{7/2}$+$^4M_{21/2}$	1.72	Moderate	$^6H_{13/2}$	455	$^6F_{5/2} + {}^6F_{5/2}$, $^6F_{1/2} + {}^6F_{7/2}$	126
Ho^{3+}	27.66 (sf)	19.52	$^5S_2 + {}^5F_4$	2.83	Moderate	$^5I_8$	547	$^5F_4 + {}^5I_7$	159, 160
			$^5I_7$	4.98	Very long	$^5I_8$	1945	No	161
Er^{3+}	27.33 (sf)	18.23	$^4S_{3/2}$	3.07	Moderate	$^4I_{15/2}$	550	$^4I_{9/2} + {}^4I_{13/2} + h\nu$	24, this work
			$^4I_{13/2}$	6.21	Long	$^4I_{15/2}$	1530	No	162, 163
Tm^{3+}	27.01 (sf)	13.47	$^1D_2$	6.29	Moderate	$^3F_4$	460	$^7G_4 + {}^3F_4 + h\nu$, $^3F_2 + {}^3H_4$	126
			$^7G_4$	6.28	Moderate	$^3H_6$	480	$^3F_2 + {}^3F_4 + h\nu$, $^3H_4 + {}^3H_5$	164
			$^3F_4$	5.70	Long	$^3H_6$	1880	No	131
Yb^{3+}	38.02	3.55	$^4F_{9/2}$	9.80	Long	$^2F_{7/2}$	980	No	165, 166

[a]The position of this level above the ground (in 10^3 cm^{-1}) versus Ce^{3+} for the same host. sf refers to a spin-forbidden excited level (exciting from the ground state). Based on Reference 56.
[b]The position of this level above the ground (in 10^3 cm^{-1}) versus Eu^{3+} for the same host. Values for Gd^{3+}, Tb^{3+}, and Ce^{3+} are greater than for Pr^{3+} (57).
[c]The minimum energy (in 10^3 cm^{-1}) that must be dissipated by phonons in a nonradiative direct relaxation.
[d]Approximate relative lifetimes at room temperature. The difference between nearest qualifiers is roughly an order of magnitude.
[e]A typical emission wavelength. Where transitions to multiple lower levels are possible, the strongest emissions are preferred. For dopants that are strongly host dependent, an approximate color is given.
[f]Assumes cross-relaxation between an ion at the emitting level and another ion at the ground state. The addition of $h\nu$ implies that one or more phonons are necessary to match the involved energy levels.

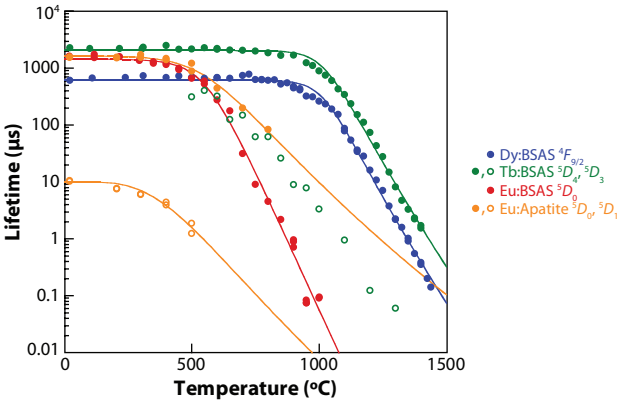

Figure 7

Fitted lifetime-versus-temperature curves for Dy, Eu, and Tb, in a modified celsian, $(Ba_{0.75}Sr_{0.25})Al_2Si_2O_8$, another proposed environmental-barrier-coating material; also, Eu in $Ca_2Gd_8(SiO_4)_6O_2$, a low thermal conductivity apatite.

Another class of oxides based on rare-earth-doped apatites of the form Ln^{3+}:$Ca_2Gd_8(SiO_4)_6O_2$ is notable for its low thermal conductivity (M. Winter & D.R. Clarke, unpublished) and high room-temperature brightness (53). Recent work on Eu:$Ca_2Gd_8(SiO_4)_6O_2$ has shown a lifetime-temperature calibration curve intermediate between (*a*) those of Eu:YSZ and Eu:BSAS on the low end and (*b*) those of Eu:Y_2SiO_5 and Eu:$Y_2Si_2O_7$ on the high-temperature end, albeit with rapidly diminishing intensity after the onset of temperature sensitivity. Interplay between the main emitting level, $^5D_0$, and the next higher, $^5D_1$, occurs through the filling of $^5D_0$ by decay from $^5D_1$. This was demonstrated to be the source of rise times observed in the $^5D_0$ emission decays. Analysis of the low-temperature measurements indicated that $^5D_0$ received a large part of its population by decay pathways through $^5D_1$, and the fairly strong emissions from $^5D_1$ contribute to the rapid loss of emission intensity from $^5D_0$ because ions that decay $^5D_1 \rightarrow {}^7F_i$ might otherwise decay $^5D_1 \rightarrow {}^5D_0$. Double-exponential decays were observed at particular wavelengths owing to overlapping $^5D_0$ and $^5D_1$ emissions (rather than the twofold site multiplicity), and the lifetime of the excited populations was demonstrated to be invariant with the excitation wavelength. Although the maximum useful temperature of this material is somewhat less than for others owing to its lower high-temperature intensity, the interactions identified underscore the richness of decay processes even in rare earths in which only a few levels are involved.

6. LUMINESCENCE OF OTHER MATERIALS

6.1. Other Yttria- and Lanthanide-Based Oxides

A number of oxides based on yttrium and the lanthanides have been studied for high-temperature luminescence. Foremost among these is $Y_3Al_5O_{12}$ (YAG), whose excellent optical and laser properties are well documented (54). Its thermometric capabilities have been studied when doped with most of the rare earths and Cr^{3+}. **Figure 8** shows the lifetime-versus-temperature curves for many of the high-temperature activators in YAG. Sm:YAG, for which lifetime data could not be found, has been reported to begin intensity quenching (which tends to coincide with or precede the temperature sensitivity of the lifetime) near 650°C and remain measurable up to at least 900°C (55). Many activators in YAG show higher temperature ranges of sensitivity than they do

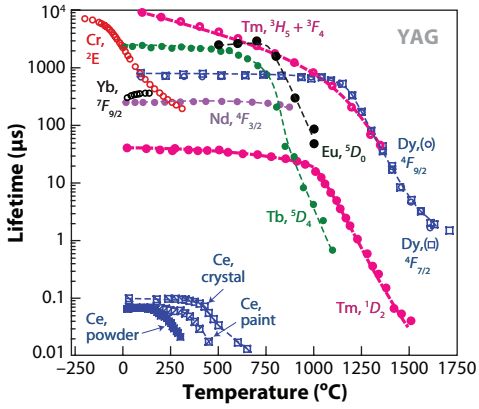

Figure 8

Luminescence lifetime versus temperature for YAG ($Y_3Al_5O_{12}$) doped with various rare earths and Cr^{3+}. Lifetimes are assigned to an emitting level (or, for one Tm:YAG curve, a mixture of emitting levels) on the basis of the observed emission wavelength. References: Tb (124), Nd (125), Dy (126), Cr (127), Ce (128, 129), YbAG (130), Tm (126, 131), Eu (based on 132, 133).

in most other materials. This may be rationalized by considering the properties of YAG: The sites on which the activators sit are low symmetry, which leads to high-intensity emissions; the positions of both the nearest CTS and $4f^{n-1}5d^1$ levels are high compared with many other hosts (see Section 8.2; 56, 57); and the most populous phonon modes are at relatively low energies (see Section 8.1). Of special note is Dy:YAG, which has been measured up to 1700°C. Other yttrium-based and yttrium-like oxides that have been studied include rare-earth ortho-aluminates (general formula: $LnAlO_3$), Y_2O_3, and YVO_4. Although these have not been examined as extensively as YAG, they generally possess good optical properties. Data for a number of these materials are presented in **Figure 9**, including those for Dy:$GdAlO_3$, which we present for the first time here (see Reference 31 for experimental details).

There are a number of interesting features of the data in **Figure 8**. Ce:YAG shows both the shortest lifetimes and the strongest sensitivity to preparation because its emission is due to a $5d^1 \rightarrow 4f^1$ transition, which is both strongly allowed and sensitive to crystal field effects. Tm:YAG shows strong emissions from several levels that are sensitive at high temperatures; the emissions from $^1D_2$ are at 350 nm and 455 nm, whereas those from $^3H_5$ and $^3F_4$ are in the infrared. Dy:YAG shows emissions up to 1700°C from both $^4F_{9/2}$ and $^4F_{7/2}$. Data for Nd:YAG were collected by looking at very small differences in lifetime and goes up only to the temperature of the onset of significant quenching but presumably could be measured further. The data for Yb^{3+}, as YbAG, demonstrate both emission at very high concentrations and an increase in lifetime with temperature probably caused by thermalization to higher-energy Stark components of $^2F_{9/2}$ that may have slower decay rates than do the lower-energy Stark components.

The calibration curves for the other oxides show a similarity of behavior for Eu^{3+} in a wide variety of oxide hosts; the onset of temperature sensitivity and the steepness of sensitivity differ depending on the host, presumably owing to changes in the energy level and Frank-Condon shift of the CTS. Tb^{3+}, as compared with its behavior in the silicates mentioned above, shows the same kind of similarity. Dy^{3+}, in contrast, shows large variations between different oxides, although the strong concentration dependence shown by Dy^{3+} makes generalization more difficult. The behavior of the $3d^3$ ions, Mn^{4+} and Cr^{3+} (in alexandrite), differ markedly between hosts, as would be expected from transition metals.

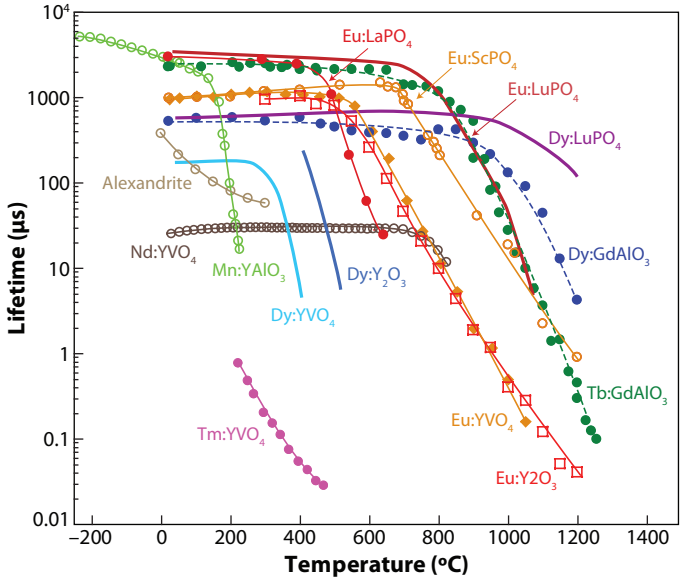

Figure 9

Luminescence lifetime as a function of temperature for a variety of other oxides. References: Alexandrite (134), Nd:YVO_4 (135), Tm:YVO_4 (3), Dy:YVO_4 (3), Eu:YVO_4 (136), Dy:Y_2O_3 (3), Eu:Y_2O_3 (136–138), Mn:$YAlO_3$ (139), Eu:$LaPO_4$ (140), Eu:$ScPO_4$ (141), Eu:$LuPO_4$ (3), Dy:$LuPO_4$ (3), Dy:$GdAlO_3$ (presented for the first time in this review), Tb:$GdAlO_3$ (31).

6.2. Alumina

The lifetimes of ruby and polycrystalline alumina have been investigated in some detail, and there are commercially available temperature sensors based on the luminescence lifetime of ruby. Typically, in these sensors a small piece of alumina or ruby is attached to the end of a fiber optic, enabling the temperature to be monitored in hostile environments, for instance, in the presence of electromagnetic radiation (Luxtron Fluoroptic® thermometry systems specifications, LumaSense Technologies, Luxtron Division). In addition, many high-temperature aluminum-containing metallic alloys form a thermally oxide (TGO) at high temperatures that is often alumina, and this TGO invariably contains sufficient chromium to yield easily measured luminescence. The range of sensitivity for Cr^{3+} is at lower temperatures than for most of the rare earths, as described in the above sections, but Cr^{3+} appears to be the only viable dopant choice for alumina. Owing to their large ionic radius, all Ln^{3+} have extremely limited solubility when substituting for Al^{3+} in alpha alumina; various recent studies put the crystal solubility limit for yttrium and the rare earths at between 0.008% and 0.001%, even near the melting temperature (58–60). This precludes fabrication of useful Ln^{3+}:Al_2O_3 sensors by most techniques. However, ion implantation could be used to form nonequilibrium sensors.

Researchers have measured lifetime-temperature calibration curves that are in good agreement up to 500°C (**Figure 10**) between single crystals, concentrations of 0.1%∼1% Cr^{3+}, and excitation at 532 nm and 514.5 nm (both are strongly absorbed) (61–64). Luminescence has been measured up to 600°C with as little as 0.1% Cr^{3+}, but above 600°C low intensity challenges further measurement. Loss of signal is the most likely reason for the discrepancy in reported lifetimes above 500°C in **Figure 10**.

Cr^{3+}, as a transition metal ion, is generally more sensitive to its crystal field environment than is Ln^{3+}. Ruby's main emitting level, ^2E, changes energy slightly with concentration, strain on

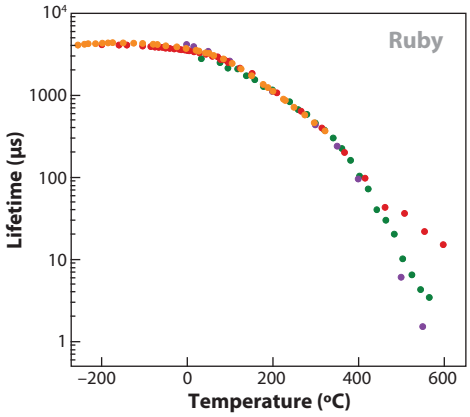

Figure 10

Luminescence lifetime as a function of temperature for Cr^{3+}-doped alumina (ruby) from four different sources (*purple*, Reference 62; *red*, Reference 63; *green*, Reference 64; *orange*, Reference 127). The scatter above 500°C is associated with loss of signal at high temperatures.

the crystal, and temperature, which causes the emission peaks to shift (e.g., ~1 nm over 600°C). The position of $^4T_2$, from which temperature sensitivity is mostly derived, changes position more rapidly with changes in the crystal field (see 65), and this can lead to changes in thermal sensitivity. For single crystals, strain along the *c*-axis is reported to have a very small effect on room-temperature lifetime (61, 66), but stress along the *m*- and *a*-axes changes lifetime significantly. Polycrystalline alumina shows similar strain sensitivity of its lifetime in both biaxial (e.g., the growth strain in TGO) and uniaxial stress states (67). We are not aware of any study that has examined the effect of strain on lifetime at high temperatures, but considering the nature of its decay pathways, the effect is probably significant.

Cr^{3+} is also very prone to concentration quenching in most hosts. In alumina the lifetime of Cr^{3+} begins to be shortened by ion-ion interactions at approximately 0.3% (68). On the basis of comparison of calibration curves from Pflitsch et al. (64) (1.1% Cr^{3+}) and Seat et al. (62) (0.1% Cr^{3+}) in **Figure 10**, such interactions may not directly affect thermalization to $^4T_2$ and, at least up to 1.1%, may only degrade intensity.

Because the main emission from $Cr:Al_2O_3$ is due to a transition to the ground state, there is a possibility of lifetime lengthening owing to efficient reabsorption of the emitted light. This has been observed in single-crystal rubies of sufficiently large size (63; see 69 for mathematical treatment) but decreases with decreasing crystal size and the use of confocal microscopes to control the area probed.

6.3. Sulfides, Halides, and Nitrides

Although this review is concerned primarily with oxides on account of their superior high-temperature stability in air, a number of doped oxysulfides, oxyhalides, and nitrides also exhibit interesting high-temperature luminescence. Except for the doped nitrides, which may fall into the category of intrinsic sensors, these materials are all extrinsic sensors with the added complication that at very high temperatures they may lose sulfur or halogen content, especially in the presence of water vapor (e.g., in a turbine engine) (70, 71). Nevertheless, a number of these doped materials are shown in **Figure 11** for reference.

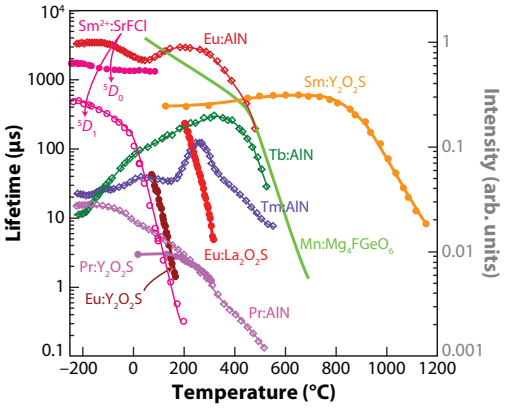

Figure 11

Luminescence lifetime as a function of temperature, as well as intensity versus temperature (where lifetime was not available), for a variety of mixed oxides, nitrides, and halides. Other than Mn^{4+} and the marked Sm^{2+}, all dopants are trivalent. References: Eu:AlN, Tb:AlN, Tm:AlN, and Pr:AlN (142); Sm:SrFCl (143); $Mn:Mg_4FGeO_6$ (3); $Eu:La_2O_2S$ (3); $Eu:Y_2O_2S$ (106) (note: this curve is based on the $^5D_2$ lifetime, not the usual $^5D_0$); $Sm:Y_2O_2S$ (144); $Pr:Y_2O_2S$ (145).

As compared with the oxides, the Eu^{3+}-doped oxysulfides show shorter lifetimes and lower temperature sensitivity. This underscores the dependence of W_{NR} for Eu^{3+} on interaction with surrounding cations through their effect on the CTS. The data for the nitrides are for intensity rather than for lifetime and provide a rough lower limit for the onset of temperature sensitivity because the quenching of intensity (which can involve filling processes as well as decay processes) usually precedes or coincides with lifetime shortening.

7. INTEGRATED SENSORS

7.1. Fabrication

Advances in materials processing now make it feasible to incorporate a luminescent dopant into the structure of a coating or component so that the sensor is integrated at the atomic level at specific spatial locations. In this way, it is possible to extend the use of luminescence thermometry from superficially applied phosphor paints to locations within a translucent coating or component where temperature measurement is required. This can be achieved by a variety of methods, such as postfabrication ion implantation (72) of the luminescent dopant, codeposition of the dopant with the coating material, and lamination during component fabrication (73, 74).

Luminescence sensors in TBCs have been incorporated in both electron-beam physical vapor deposition (EB-PVD) and air plasma spray (APS) TBCs. In the former, segmented ingots with the dopant in one of the segments may be used so that a sensor layer of doped material is included during the coating process at a depth (5, 75) and thickness determined by the position and thickness of the doped ingot segment. The 10-µm-thick Eu-doped sensor layer shown in the micrograph in **Figure 12** was prepared in this manner. Alternatively, the dopant can be introduced at the desired depth with a multiple-source EB-PVD system, as was done for sensors described in other works (73, 74). In APS TBCs, luminescence layers (and structures) can be introduced by modulating the powder feedstock during thermal spraying (76).

Extrinsic sensors—sensors that are formed in an additional processing step and that may be made of different materials than the component to which they are added—may be deposited by

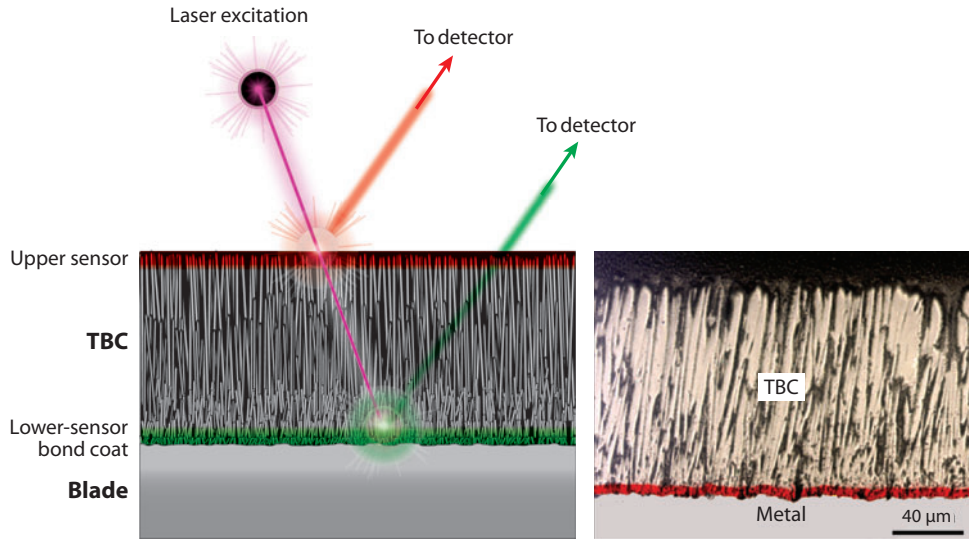

Figure 12

(*Left*) A schematic of a sensor system designed to measure thermal gradients directly. (*Right*) A scanning electron microscope (SEM) image overlaid with a cathodo-luminescence image of a buried Eu:7YSZ layer at the bond-coat surface of a 7YSZ thermal barrier coating (TBC) (deposited by electron-beam physical vapor deposition). The buried Eu-doped layer luminesces red in the cathode-luminescence image.

a great number of techniques, including APS (76), EB-PVD (73, 74), pulse laser ablation (3), spray pyrolysis (77), slurry coating and sintering (with or without a binder) (78), and sputtering (3). The reader is referred to the review by Allison (3) for a fuller discussion of these approaches.

For TBCs the temperature at the base of the coating, in contact with the underlying alloy, is of particular concern. This is because the oxidation rate of the metal depends exponentially on temperature, and a difference of a few degrees can change the lifetime of a TBC significantly through an increase or a decrease in the rate of oxide growth and subsequent spallation. Typical TBCs have thicknesses between 140 μm (EB-PVD) and 3 mm (APS), so coating surface temperature measurements are not very informative when the coatings support a steep thermal gradient, as in engine use. The use of a 10-μm Eu-doped YSZ sensor for thermometry in a standard EB-PVD coating has been demonstrated in isothermal conditions (79) and in temperature gradients (80) over a range of temperatures.

With two sensors located at different depths in a coating, it is, in principle, possible to directly measure the thermal gradient between the sensors and to calculate the heat flux without adding any thermal mass to the coating. For such a system the two sensors must be based on different activators. Each sensor may then be interrogated separately, by virtue of nonoverlapping excitation peaks, or else, if the activators have nonoverlapping emission peaks, the temperatures of the two sensor layers may be measured simultaneously. **Figure 12** shows a diagram of such a sensor system in cross section. The use of such multilayers extends beyond turbine engines, of course, and has been demonstrated in luminescence wear sensors (81).

Integrated silicate sensors for application in EBCs have not, to our knowledge, been evaluated yet. Because the crystallization kinetics of refractory silicates are, in general, slower than those for zirconia and related materials, additional processing steps to crystallize them may be necessary to produce a stable and reproducible sensor.

7.2. High-Temperature Stability

The long-term stability of luminescence sensors at high temperatures is an important practical consideration. Provided that the activator is below the solubility limit—which can be quite high when it is a Ln^{3+} substituting for either Y^{3+} or another Ln^{3+}—an intrinsic sensor would be expected to be indefinitely stable, except in the case of a host that was itself only metastable (e.g., YSZ, addressed above). However, diffusion may still tend to delocalize a well-defined sensor layer into the surrounding material, causing information to come from a larger volume than intended. The significance of this effect will depend on the specific host and dopant and the temperature gradient across the sensor. However, the diffusivities of rare-earth ions in the oxides of interest, where they have been measured, are usually very small. For instance, the lattice diffusivity of Y^{3+} in YSZ is less than 10^{-15} cm^2 s^{-1} at 1200°C (82). Faster grain boundary diffusion will also occur, but nevertheless a 10-μm-thick sensor would remain essentially the same thickness even after 1000 h at 1200°C, longer than the expected life of any turbine engine component at such an operating temperature.

The effect of concentration variations within a sensor may also be a concern if the activator is concentration dependent. Even though most high-temperature sensor materials investigated to date have included dopants well below the onset of concentration quenching, intensity does not begin to decrease with concentration until after the lifetime has begun to be affected. Sufficiently low dopant concentrations can reduce the uncertainty associated with concentration variations because, below some threshold, lifetimes are concentration independent. Additionally, not all activators depend on concentration to the same degree; see Section 8.

Of greater concern is the long-term stability of extrinsic sensors, materials deposited on the surfaces of components with different composition, the functional equivalent of thermographic paints. If one can choose a sensor material that is in thermochemical equilibrium with the component or if one can use a barrier oxide between the sensor and component that is in equilibrium with both, the requirement of compatibility is largely met. For instance, from known phase diagrams $GdAlO_3$ is stable with respect to both $Gd_2Zr_2O_7$ TBCs and Al_2O_3, which is grown upon oxidation of most high-temperature alloys (83). Similarly, YAG and rare-earth phosphates (e.g., monazite, $LnPO_4$) are also stable with respect to Al_2O_3 (84), and Y_2O_3 is stable with respect to $Y_4Zr_3O_{12}$, another low-thermal-conductivity oxide (85). But except for such combinations, it is likely that most sensor layers will react with the component onto which it is applied. Whether the reaction is prohibitive will depend on its kinetics and the luminescent properties of the reaction phases formed.

8. NONRADIATIVE DECAY PROCESSES

In this section, we describe the principal nonradiative processes by which the excited state can decay and how they depend on temperature and the energy level structure of the luminescing ions. This is of importance because, although many of the lifetime-temperature curves look superficially similar—a flat regime of nearly constant lifetime followed by an exponential decrease in lifetime at higher temperatures—several different nonradiative processes can give rise to similar temperature sensitivity. The identification of which nonradiative process governs the high-temperature lifetime of a given material—that is, the identification of which nonradiative process depopulates the excited state most quickly—depends on the analysis of the shape of the calibration curve and knowledge of which processes, for a given sensor material, are feasible.

8.1. Direct Relaxation

The conceptually simplest nonradiative process is the transition from one excited level to a lower level, with the extra energy being dissipated into phonons rather than photons (86) (see **Figure 1**).

Because most strongly emitting levels have no levels close beneath them, more than one phonon is usually required; therefore, this process is often called MPR. Unlike radiative transitions, the rate of this process depends on the energy being expended. According to Riseberg & Moos (87),

$$W_{ij}^{MP}(T) = W_0^{MP}\left(\frac{1}{\exp(h\nu/kT)-1}+1\right)^{\Delta E/h\nu}. \qquad 6.$$

W_0 is usually used as a fitting term, although rigorously it depends on electron-lattice coupling strength and symmetry terms relating to the crystal field and the phonon modes. $h\nu$ is the energy of the phonons involved in the process. A more rigorous approach would account for an ensemble of phonons with different energies, symmetries, and population densities, but $h\nu$ is often approximated to have a single value. The value of ΔE is the gap between the initial level, i, and the final level, j; thus, $\Delta E/h\nu$ is the number of phonons involved in the decay process. The rate, W_{MP}, depends strongly on ΔE. Thus, very often one considers only the next lower level from the excited state because decay to that level (by this process) will be much faster than decay directly to lower levels. Minimum values for ΔE are given in **Table 1** for the important emitting levels of the rare earths.

8.2. Charge-Transfer and $4f^{n-1}5d^1$ States

One characteristic aspect of the energy levels of Ln^{3+} ions is that $4f$ energy levels are all similarly dependent on their configuration coordinate, the position of the oxygen ions around the ion (often approximated as the breathing mode). This means that it is not possible for two different $4f$ configurations to become degenerate by a perturbation of the configuration, a process that could otherwise facilitate radiationless transition from a higher level (at the Frank-Condon minimum) to a lower level.

There are two excited states for rare earths, generally at fairly high energies, which do have Frank-Condon shifted minimum configurations and can form radiationless decay pathways between $4f$ states. The first is a CTS that, for rare earths in oxides, corresponds to the temporary transfer of an electron from the coordinating oxygen to the metal ion. The second is the promotion of $4f$ electrons out of the $4f$ shell, in particular to a $4f^{n-1}5d^1$ state; this state is no longer shielded by the $5s$ and $5p$ electrons and consequently interacts strongly with the crystal field. These states are often involved in excitation (see **Figure 13**) because most of them are highly allowed transitions that absorb incident light efficiently, then decay rapidly to the longer-lived $4f$ states. They can also play a role in nonradiative decay by acting as a pathway between the $4f$ states (see **Figure 14*a***). There is an energy barrier, E_a, between the $4f$-state minimum and its crossover point with the CTS (or $4f^{n-1}5d^1$ state). After this barrier is surmounted, the ion may decay rapidly to a lower-lying level (88, 89). A multidimensional quantum mechanical treatment of the process has been made (90), and the rate equation for this process is

$$W_{CT}(T) = W_0 T^{*-1/2}\exp(-E_a/kT^*), \qquad 7a.$$

where

$$T^* = (h\nu/2k)\coth(h\nu/2kT). \qquad 7b.$$

Here $h\nu$ has the same meaning as for direct relaxation. Excitation spectroscopy yields information about the energy of the CTS for the ion in its equilibrium configuration, but deducing the shape of the CTS may require careful studies of emissions (88, 89), lifetimes, and branching ratios. Nevertheless, some general trends can be outlined, and for Ln^{3+} one may anticipate whether a CTS or a $4f^{n-1}5d^1$ state is likely to be at low enough energies to be important. The positions of

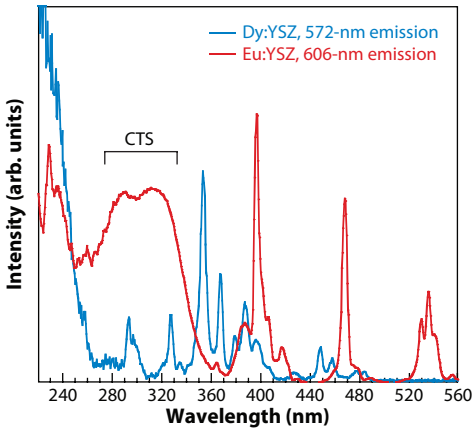

Figure 13

Excitation spectra for Eu:YSZ and Dy:YSZ showing a combination of sharp peaks associated with the energy levels of the rare earths and, for Eu^{3+}, the presence of a broad, intense charge-transfer (CT) excitation band between 280 nm and 340 nm.

these states depend strongly but fairly systematically on the host; **Table 1** provides relative values for their positions above the ground state. For Tb^{3+} through Tm^{3+}, the lowest-energy $4f^n \rightarrow 4f^{n-1}5d^1$ transitions are spin forbidden. These forbidden transitions are more difficult to observe in absorption or emission spectroscopy but cannot be ignored as possible decay pathways. The values given in **Table 1** correspond to the lowest $4f^{n-1}5d^1$ state, whether or not transition to it from the ground state is allowed. The value of E_a, then, depends on the host-dependent position of the CTS or $4f^{n-1}5d^1$ level, the position of the emitting level of interest, and the host-dependent configuration-energy curves of both states.

8.3. Thermalization

At high temperatures there may be sufficient thermal energy to excite ions from one level to a slightly higher level, which can lead to effects in both excitation and decay properties. One example is Eu^{3+}, for which the $^7F_1$ level is significantly populated from the ground state, $^7F_0$, even at room temperature (20), and whose population causes increased absorption of 532-nm excitation with temperature (532 nm more closely matches $^7F_1 \rightarrow {}^5D_1$ than $^7F_0 \rightarrow {}^5D_1$). Another is the case of Dy:$YAl_3(BO_3)_4$, for which the luminescent lifetime increases from 10 K to 298 K, caused by the promotion of lower Stark components within the excited state to longer-lived, higher-energy Stark components (91).

Thermalization is particularly important for $3d^3$ transition metals. In Cr:Al_2O_3 the high-temperature lifetime of the emitting level, ^2E, is governed by thermal promotion to $^4T_2$, which decays rapidly to the ground state by a strongly allowed transition (4) (**Figure 14*b***). A general equation based on the Maxwell-Boltzmann distribution can be easily derived to describe the observed lifetime with an arbitrary number of interacting levels, using W_i to describe the decay rates of each level, g_i to describe the degeneracy of each level, and ΔE_i to describe the gap between the base level, 0, and level i:

$$W_{observed} = \sum_{i=0} \left[W_i \frac{g_i \exp(-\Delta E_i/kT)}{\sum_{j=0} g_j \exp(-\Delta E_j/kT)} \right]. \quad 8.$$

Figure 14

(*a*) Schematic illustration of the decay process for Eu^{3+} through an intermediate charge-transfer state (CTS). Temperature dependence is based on the thermal activation of the excited state over the barrier, E_a, to the CTS. (*b*) Illustration of thermalization-assisted decay in a $3d^3$ ion; long-lived ^2E becomes increasingly coupled to short-lived $^4T_2$ at high temperatures according to the Maxwell-Boltzmann distribution of the excited ^2E population. (*c*) Schematic of a cross-relaxation process (*solid arrows*) for Dy^{3+} followed by subsequent decay (*dashed arrows*). The process depends on temperature through the imperfect energy matching of the transitions involved.

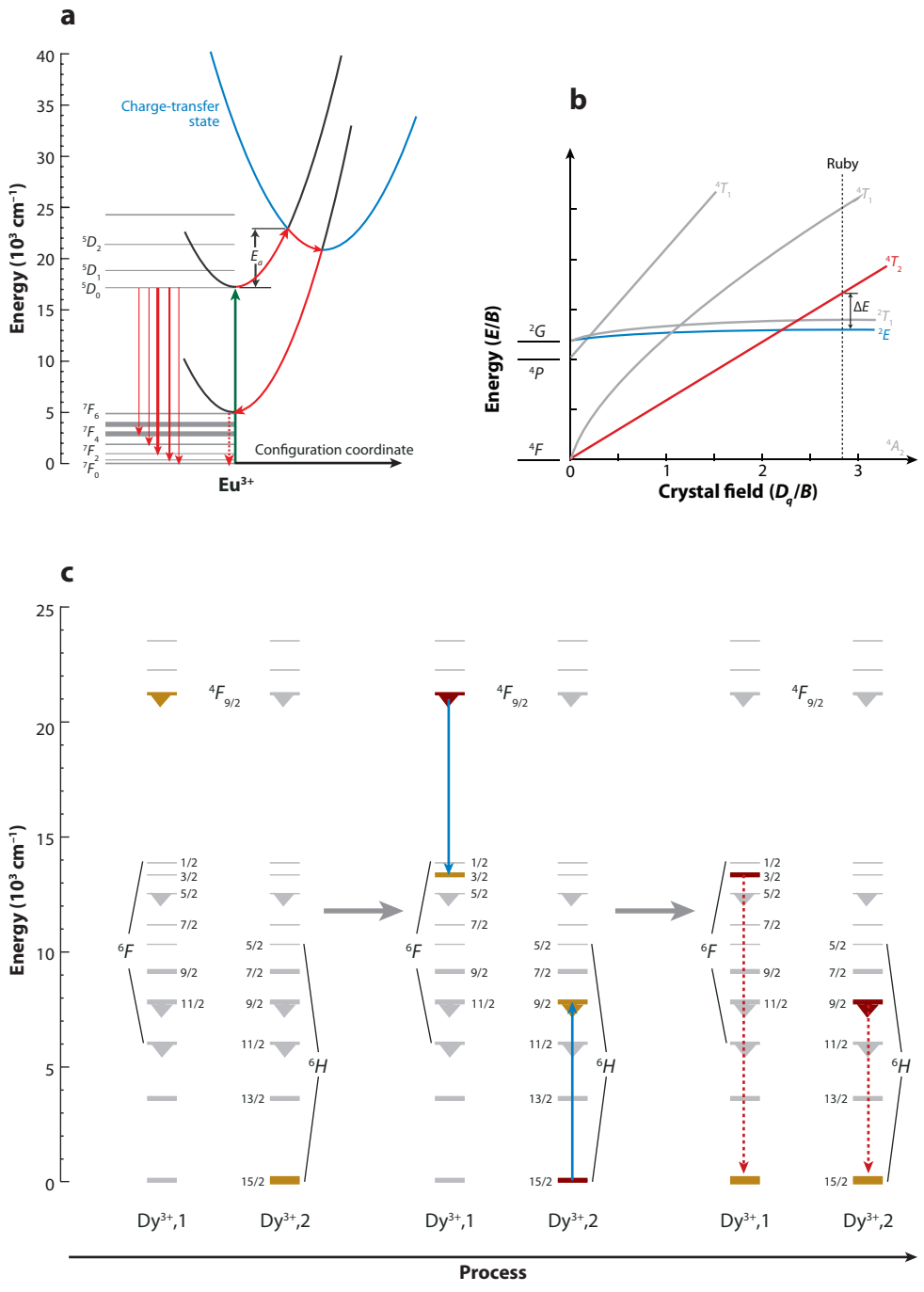

8.4. Energy Migration and Cross-Relaxation

With increasing dopant concentration, the spacing between dopants decreases, and ions with appropriately matched energy levels can couple and efficiently transfer energy from one to another (see References 92 and 93 for a description). In the case of a single available excited state, this can lead to energy migration from one dopant ion to another along a chain of closely spaced dopants. Energy migration does not affect lifetime directly, but certain defects and impurities (quenching centers) can facilitate nonradiative decay and strongly affect lifetime, even in very small concentrations. The effect of energy migration on lifetime depends strongly on the concentration of the activator and also on the relative rates of emission and migration. Weber (94) has quantitatively described a number of scenarios, including situations in which the effect is strongly temperature dependent.

In the case where there are many available excited states, another process can occur: the incomplete transfer of energy from an excited ion to an unexcited ion, leading to two ions excited to intermediary levels between the initial excited state and the ground state (**Figure 14*c***). Often these intermediary levels have short lifetimes and decay back to the ground state by some other means. This process is called cross-relaxation. Like energy migration, cross-relaxation is concentration dependent, but not all energy levels can decay by cross-relaxation. For instance, the $^5D_0$ level of Eu^{3+} cannot undergo cross-relaxation because there are no intermediary levels between $^5D_0$ and the ground that can between them account for all the $^5D_0$ energy. In contrast, the $^4F_{9/2}$ level of Dy^{3+} undergoes cross-relaxation readily, for instance, by

$$^4F_{9/2} + {}^6H_{15/2} \rightarrow {}^6F_{3/2} + {}^6F_{11/2}. \quad 9.$$

In concentrations as low as 12% (cation), Dy^{3+} may be completely nonluminescent. Activators that cannot cross-relax, in contrast, can luminesce in high concentrations such as in $Eu(PO_3)_3$, $Eu_2Zr_2O_7$, and $TbAlO_3$ (10, 94, 95). Besides contributing to concentration quenching of intensity (see 96, 97) and shortening the room-temperature lifetime, cross-relaxation can also be temperature dependent. Cross-relaxation of Nd^{3+}, for instance, according to

$$^4F_{3/2} + {}^4I_{11/2} \rightarrow {}^4F_{5/2} + {}^4I_{15/2} + h\nu \quad 10.$$

is an inexact energy balance and requires some extra amount of energy to be dissipated. The temperature dependence of the process arises from the availability of phonons to absorb or add the extra energy necessary to balance the equation. **Table 1** provides possible cross-relaxation mechanisms for many of the important emitting levels for the rare earths.

9. PROCEDURES FOR DECAY ANALYSIS AND TEMPERATURE DETERMINATION

9.1. Decay Phenomena

As mentioned above, luminescence decays are rarely simply exponential in character except for an ideal sensor, and so detailed analysis of the decays is essential for determining temperature as well as for identifying possible decay mechanisms. In many oxides the character of the decay can be more complex. Much of the complexity arises from the simultaneous excitation and emissions of multiple populations; the processes W_{NR} and W_R for every excited level (within a single population) are independent of how that level was populated, i.e., of the excitation wavelength. For instance, overlapping emissions from multiple levels or emissions from different populations (i.e., Ln^{3+} sitting on two different crystallographic sites) can lead to double-exponential or higher-order decays. In these cases it is usually the longest decay that is plotted in lifetime-temperature calibration curves

for high-temperature measurement, such as in **Figures 4** and **6–11**. Activators that can undergo cross-relaxation or significant energy migration to quenching sites often show a continuous distribution of lifetimes, or curved exponential decays. Furthermore, activators with slow-decaying levels above the main emitting level can show rise times at the beginning of their decays as the upper level decays to fill the lower (e.g., 98, 99). The character of a material's decay is also often temperature dependent. Although these different components of a decay provide additional information about the electronic processes in a material and can often expand the window of temperature sensitivity, they sometimes require careful handling to achieve precise values for the lifetime.

9.1.1. Multiexponential decays. Multiexponential decays represent the sum of two or more single-exponential decays and can be fit simply by adding more terms to Equation 2b:

$$I(t) = \sum_i I_i \exp\left(\frac{-t}{\tau_i}\right). \qquad 11.$$

However, all non-single-exponential decays must be fitted in log space because fits in linear space underestimate the error for low-value data points. (This artifact can even affect single-exponential decays with large amounts of noise by deflecting the fit toward the top of the scatter.) An example of a suitable nonlinear least-squares fitting method is the optimization of a Pearson's R by the Levenberg-Marquardt algorithm:

$$R = \sqrt{1 - \frac{\chi^2}{\sum_i \left(\log y_i - \overline{\log y}\right)^2}}, \qquad 12a.$$

where

$$\chi^2 = \sum_i (\log y_i - \log f(x_i))^2. \qquad 12b.$$

x_i and y_i represent the time and intensity values of the points on the trace respectively, $f(x_i)$ is the value of intensity from the fitting equation for time x_i, and $\overline{\log y}$ is the average of the logarithm of all intensity values.

This approach greatly improves the fit of decays with more complex character than single exponential, though it has two shortcomings. First, any very fast decays will be poorly fitted because, with linear time sampling, there will be fewer data points associated with them. Second, negative values and zeros must be discarded because they cannot be represented in log space. This practice either limits the length of a decay trace that can be fit, or requires fitting the background as well (rather than the preferred method of measuring and subtracting the background).

9.1.2. Curved decays. Decays with curved character present the challenge of defining a characteristic lifetime value from a continuous distribution of lifetimes. Achieving a satisfactory fit is usually possible with either an empirical equation, such as the Kohlrausch-Williams-Watts equation, a stretched exponential,

$$I = I_0 \exp\left(-\left(\frac{t}{\tau}\right)^{1/\Gamma}\right), \qquad 13.$$

or an equation with a physical meaning, such as the energy migration equations of Weber (94):

$$I = I_0 \exp\left[\frac{-t}{\tau} - c\left(\frac{t}{\tau}\right)^d\right]. \qquad 14.$$

However, the value of τ is highly sensitive to noise and generally cannot be compared across different equations. One way to increase the reproducibility of lifetime values derived from such data is to define the characteristic lifetime as the instantaneous lifetime (that is, the inverse of the instantaneous decay rate) at a set point along the decay, e.g., −20 dB. From the derivative of Equation 2b, it is simple to show that this value is equal to

$$\tau_{20\,\mathrm{dB}} = \frac{-I(t_{20\,\mathrm{dB}})}{(dI(t_{20\,\mathrm{dB}})/dt)}. \qquad 15.$$

The advantage of this approach is that arbitrarily complex fits can be used as long as *dI/dt* is smooth near the point of interest. The value of $t_{20\,\mathrm{dB}}$ may be calculated numerically with ease. The main disadvantage of this approach is that it is sensitive to artifacts at the beginning of the decay (e.g., spikes from stray luminescence), which may effectively offset the position of $t_{20\,\mathrm{dB}}$.

9.1.3. Rise times. The filling of the emitting level is usually fast, but if there is a fairly long-lived level above the emitting level that is also excited, an initial rise of intensity can be observed and its rise time measured. The intuitive, empirical equation used to fit such a decay curve is

$$I(t) = \left(I_2^* \cdot \exp\left(\frac{-t}{\tau_2^*}\right) + I_1\right) \cdot \exp\left(\frac{-t}{\tau_1}\right). \qquad 16.$$

Here, τ_2^* is generally taken to be the lifetime of the filling level (level 2) and τ_1 the lifetime of the emitting level (level 1). However, this is not exactly correct. For a system in which level 2 decays to level 1 at rate W_{21}, in which level 2 decays (overall) at rate W_{2x}, and in which level 1 decays at rate W_{1x}, the governing differential equations are

$$\frac{dN_2}{dt} = -N_2 \cdot W_{2x}$$
$$\frac{dN_1}{dt} = -N_1 \cdot W_{1x} + N_2 \cdot W_{21}. \qquad 17a,b.$$

The solution to these equations requires the introduction of initial populations of levels 1 and 2, N_1^0 and N_2^0:

$$I(t) \propto N_1(t) = \left(\frac{N_2^0 \cdot W_{21}}{W_{1x} - W_{2x}} \cdot \exp[-t \cdot (W_{2x} - W_{1x})] + N_1^0\right) \cdot \exp(-t \cdot W_{1x}). \qquad 18.$$

Thus, τ_2^*, the rise time, depends on the lifetimes of both the upper and lower populations, although for $W_{2x} \gg W_{1x}$ the values of τ_2^*, the rise time, and τ_2, the real lifetime of the upper level, are similar.

9.1.4. Frequency-domain measurements. Lifetimes can also be calculated in the frequency domain with similar precision, as described in detail elsewhere (100, 101). However, the decay character is masked in this approach, and the measurement of transient temperatures or rapidly moving surfaces is precluded.

9.2. Temperature Sensitivity and Precision

The temperature-sensitive range of a luminescent material can be limited at high temperatures by shortness of the decay time (i.e., beyond that of the excitation or detection equipment's capabilities) or by loss of intensity. However, the intensity relevant to lifetime thermometry is not the same as that relevant to spectroscopy. In spectroscopy, the signal that follows an excitation pulse is equal

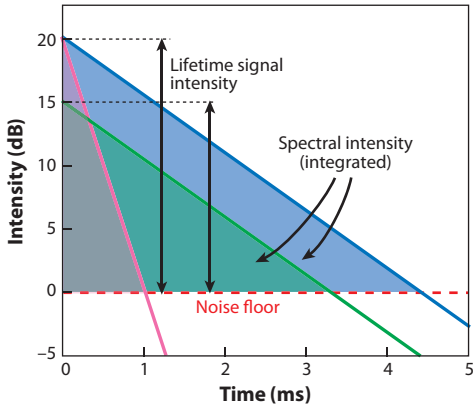

Figure 15

Schematic of three different signals (*blue*, *green*, and *pink*) to illustrate the difference between lifetime signal strength and spectral signal strength. Both the blue and pink decays have the same initial intensities (which is important to lifetime measurement) but different integrated intensities (which is important to spectral measurement). The green decay has a weaker lifetime signal but a stronger spectral signal than the pink decay.

to the integrated area under the decay curve:

$$I_{spectral} = \int I(t)\,dt = \tau \cdot I_0. \qquad 19.$$

That is, as W_{NR} increases and lifetime decreases, I decreases. However, in lifetime thermometry the signal is equal to the length of the decay trace (expressed in decibels, not time) before it reaches the noise background (which is additive in nature)—that is, the initial height of the decay trace:

$$I_{decay} = N_0 \cdot W_R. \qquad 20.$$

In contrast to the spectroscopy considerations, this signal is not affected by an increase in W_{NR} as expressed schematically in **Figure 15**. The two primary factors that degrade the signal-to-noise ratio with increasing temperature are, instead, the increase in background noise associated with black-body radiation and possible decreases in N_0—for instance, changes in the branching ratio after excitation to a CTS.

There is also noise in the data points of a decay trace that is at least semimultiplicative in nature. This noise has to do with statistical sampling and depends on the total number of photons collected (Equation 19), as well as on electronic noise in the collection system and a number of other things. It does not affect the ability to make a measurement as can large amounts of additive noise, but it does affect the precision of fitted lifetime values.

A full discussion of the effect of noise in decay traces is highly involved and not offered here. Nevertheless, the multiplicative noise, MN, and the number of decay traces that are averaged together, n, both go into the final precision of the lifetime extracted from a decay trace. The precision in temperature, ΔT, that can be measured depends on the precision of the lifetime and also on the steepness of the calibration curve:

$$\Delta T \propto \left(\frac{d\tau}{dT}\right)^{-1} \Delta\tau\left(MN, \sqrt{n}\right). \qquad 21.$$

Thus, the value of $d\tau/dT$ is an important aspect of the calibration curve for any material because it directly affects the precision of a temperature measurement. Although a sharper fall-off

of lifetime with temperature tends to limit the range of temperature sensitivity for that material, it leads to more precise values of T over that range.

Another factor comes into play when measuring temperature in a large temperature gradient, namely the temperature variation through the thickness of the sensor, h. If the temperature gradient is dT/dx, then the finest temperature precision that can be measured directly is $h \cdot dT/dx$. The temperature gradients in gas turbine blades can be particularly high, of the order of $\sim 0.5°C\ \mu m^{-1}$ at 1000°C (5), so a 10-μm sensor is limited to measuring temperatures to +/−2.5°C, an impressive accuracy nonetheless. For more common gradients this effect is not likely to be limiting, and several authors have presented analytical techniques to deconvolve lifetimes from such distributions (102–104).

Measurement on moving components (e.g., turbine blades) can impose an additional, lower temperature sensitivity limit. Such moving parts may be visible to the optics of the interrogation system for only a short period of time, which imposes an upper lifetime limit (5). Systems that are thermally dynamic may impose a limit on n, the number of decay traces that can be collected, which limits the precision that can be achieved. Nevertheless, measurement on both stationary surfaces [e.g., an afterburner (105)] and rotating surfaces (106, 107) has been demonstrated.

9.3. Measurements in Real Time

For laboratory characterization work, the application of a minimization algorithm (such as the Levenberg-Marquardt, described above) to fit decays is sufficiently fast. However, to make real-time temperature measurements, a faster approach may be required in some circumstances. Instead of a nonlinear least-squares fit, an autoregressive model may then be necessary. For treating decays with complexity greater than single-exponential character, the most popular approach, referred to as Prony's method, is to express $I(t)$ as a recursive equation (108):

$$I(t) = \sum_{i=1}^{M} B_i I(t - i\Delta t), \qquad 22.$$

where B_i are fitting terms. Work by Sasaki & Masuhara (108) offers an improvement in the accuracy of the fit by including consideration of convolutions, and Enderlein & Erdmann (109) have described further refinements. The advantage of these approaches is speed of fit, but they are less accurate than nonlinear least-squares regressions. The reader is referred to these works as well as those of Novikov (110), Zhang et al. (111), and Rosso et al. (101) for a fuller description of the mathematical treatment of these fits as well as of other fitting techniques.

10. OUTLOOK

Advances in luminescence lifetime thermometry over the past decade have identified a large number of oxides that can be used as both intrinsic and extrinsic sensors and that cover a wide range of temperatures with sensitivities ranging from low temperatures up to at least 1700°C. These include oxides with technologically important applications such as TBCs and EBCs for use in both ground-based power generation and aerospace gas turbine engines. The study of other high-temperature materials, such as the silicates and nitrides, has only recently begun, and similar developments can be expected. Moreover, there are a growing number of studies on sensitizers at room temperature, which can greatly improve excitation efficiency (e.g., 112, 113). They may likely be employed at high temperatures as well to increase the high-temperature sensitivity of many intensity-limited sensor oxides.

Numerous applications for thermometric sensor layers exist beyond TBCs and are expected to proliferate as oxides are increasingly being used at high temperatures. For instance, the use of two or more layers to measure thermal gradients and thus thermal conductivity is applicable outside of the TBC materials for which the concept was described here. Walker (114) has described an arrangement using a single-layer sensor to measure heat flux (although not thermal gradient). Omrane et al. (115) and Brubach et al. (116) have used luminescence thermometry to measure combustion surfaces and thermal spray profiles, respectively, and Allison et al. (117) have used luminescent sensors to measure the heating of railgun armatures during firing (albeit at much lower temperatures than seen with TBCs so far). There is also the prospect of using luminescence thermometry to measure temperatures in high-temperature thermoelectrics and in oxide-based catalysis systems in which noncontact monitoring is necessary. Moreover, the same properties that lead to long lifetimes at high temperatures (i.e., the retardation of W_{NR} processes) also lead to high brightness at high temperatures, and good high-temperature sensor materials also make good high-temperature phosphors in general.

Luminescent sensor layers may be used, either separately or in conjunction with thermometry, for purposes such as wear sensors (81), erosion sensors (9, 75), and delamination sensors (74). Radiation damage sensing may also be possible on the basis of the degradation of luminescence through knock-on damage or the introduction of quenching centers (for instance, color-center defects). Other applications, and the need for different materials, will doubtless arise as energy systems are designed for increasingly high-temperature operation.

FUTURE ISSUES

1. As illustrated in this review, a wide variety of rare-earth ions can be incorporated into several oxides of varying structural complexity and can give strong luminescence up to high temperatures. However, despite the similarity in the variation of luminescence lifetime with temperature between many materials, there are several different processes, W_{NR}, that operate at high temperatures (see Section 7). The processes depend on the activator, the host, and the concentration of the activator (as well as on any important impurities or crystal defects present). A deeper understanding of the interplay between host and dopant is needed to engineer sensors with optimal properties and to fully realize their potential. Whereas W_R can be predicted fairly well by the Judd-Ofelt theory (118, 119), there is insufficient understanding to predict the rates and temperature dependencies of all W_{NR} processes, requiring a tedious experimental approach to identify suitable sensor materials for a given application.
2. There is a need for extending the sensitivity to even higher temperatures than has been reported for current zirconia sensor materials used in thermal barrier coatings and related applications. Improvements in luminescent yield, for instance, by the use of sensitization, or in signal collection efficiency, for instance, by time-correlated single-photon counting (TCSPC), could overcome this.
3. The precision to which temperature can be measured by luminescence decays is very often limited by the distribution in lifetimes represented in any measured decay. The ability to rigorously analyze a decay and to deconvolve the lifetime spectrum that composes it would greatly improve temperature precision and assessments of precision as well as potentially yield rich information about the distribution of dopant ions and defects in a material. A rigorous analysis of the individual contributions to noise in a lifetime measurement system is also needed.

4. Researchers have identified a number of sensor materials with excellent high-temperature properties that could be used as extrinsic sensors, but the stability of sensor layers based on these materials, and their effect on the system in which they are introduced, still needs rigorous study if they are to be implemented in systems with long expected lifetimes. In contrast, changes in luminescent lifetime may being a practical tool for nondestructively monitoring the early stages of chemical reaction between oxides at high temperatures.

DISCLOSURE STATEMENT

The authors are not aware of any biases that might be perceived as affecting the objectivity of this review.

ACKNOWLEDGMENTS

The authors would like to thank Dr. Bauke Heeg of Metrolaser, Dr. Katsuhisa Tanaka of Kyoto University, and especially Dr. Jeff Eldridge of the NASA Glenn Research Center for their insightful discussion. We would also like to thank Dr. Eldridge, as well as Dr. Steve Allison of Oak Ridge National Laboratory, for assistance in obtaining some of the data contained in this work and Paul Rousseve for the preparation of several of samples from which data presented here were collected. This work has been supported by the National Science Foundation, the Office of Naval Research, and a National Defense Science and Engineering Graduate (NDSEG) Fellowship held by the first author.

LITERATURE CITED

1. Childs PRN, Greenwood JR, Long CA. 2000. Review of temperature measurement. *Rev. Sci. Instrum.* 71:2959–78
2. Bradley LC. 1953. A temperature sensitive phosphor used to measure surface temperatures in aerodynamics. *Rev. Sci. Instrum.* 24:219–20
3. Allison SW, Gillies GT. 1997. Remote thermometry with thermographic phosphors: instrumentation and applications. *Rev. Sci. Instrum.* 68:2615–50
4. Grattan KTV, Zhang ZY. 1995. *Fiber Optic Fluorescence Thermometry*. London: Chapman & Hall
5. Gentleman MM, Lughi V, Nychka JA, Clarke DR. 2006. Noncontact methods for measuring thermal barrier coating temperatures. *Int. J. Appl. Ceram. Technol.* 3:105–12
6. Omrane A, Ossler F, Alden M. 2002. Two-dimensional surface temperature measurements of burning materials. *Proc. Combust. Inst.* 29:2653–59
7. Blasse G. 1992. Rare earth spectroscopy in relation to materials science. *Mater. Chem. Phys.* 31:3–6
8. Feist JP, Heyes AL. 2000. Europium-doped yttria-stabilized zirconia for high-temperature phosphor thermometry. *Proc. Inst. Mech. Eng.* 214:7–12
9. Gentleman MM, Clarke DR. 2004. Concepts for luminescence sensing of thermal barrier coatings. *Surf. Coat. Technol.* 188–189:93–100
10. Gentleman MM, Clarke DR. 2005. Luminescence sensing of temperature in pyrochlore zirconate materials for thermal barrier coatings. *Surf. Coat. Technol.* 200:1264–69
11. Gutzov S, Assmus W. 2000. The luminescence of holmium doped cubic yttria-stabilized zirconia. *J. Mater. Sci. Lett.* 19:275–77
12. Alonso PJ, Alcala R, Casas-Gonzalez J, Cases R, Orera VM. 1989. Spectroscopy of chromium (III) in yttrium-stabilized ZrO_2. *J. Phys. Chem. Solids* 50:1185–91

13. Merino RI, Orera VM, Cases R, Chamarro MA. 1991. Spectroscopic characterization of Er^{3+} in stabilized zirconia single crystals. *J. Phys. Condens. Matter* 3:8491–502
14. Ping L, Chen IW. 1994. Effect of dopants on zirconia stabilization: an X-ray absorption study. I. Trivalent dopants. *J. Am. Ceram. Soc.* 77:118–28
15. Yugami H, Koike A, Ishigame M, Suemoto T. 1991. Relationship between local structures and ionic conductivities in ZrO_2-Y_2O_3 studied by site-selective spectroscopy. *Phys. Rev. B* 44:9214–22
16. Dexpert-Ghys J, Faucher M, Caro P. 1984. Site selective spectroscopy and structural analysis of yttria-doped zirconias. *J. Solid State Chem.* 54:179–92
17. Merino RI, Orera VM, Povill O, Assmus W, Lomonova EE. 1997. Optical and electron paramagnetic resonance characterization of Dy^{3+} in YSZ single crystals. *J. Phys. Chem. Solids* 58:1579–85
18. Merino RI, Orera VM. 1993. Site resolution spectroscopy of Nd^{3+} in yttrium stabilized zirconia. *Solid State Commun.* 88:435–38
19. Bazzi R, Flores MA, Louis C, Lebou K, Zhang W, et al. 2004. Synthesis and properties of europium-based phosphors on the nanometer scale: Eu_2O_3, Gd_2O_3:Eu, and Y_2O_3:Eu. *J. Colloid Interface Sci.* 273:191–97
20. Chambers MD, Rousseve PA, Clarke DR. 2008. Luminescence thermometry for environmental barrier coating materials. *Surf. Coat. Technol.* 203:461–5
21. Shen Y, Chambers MD, Clarke DR. 2008. Effects of dopants and excitation wavelength on the temperature sensing of Ln^{3+}-doped 7YSZ. *Surf. Coat. Technol.* 203:456–60
22. Weber MJ. 1967. Selective excitation and decay of Er^{3+} fluorescence in LaF_3. *Phys. Rev.* 156:231–41
23. Weber MJ. 1967. Probabilities for radiative and nonradiative decay of Er^{3+} in LaF_3. *Phys. Rev.* 157:262–72
24. Tanabe S, Suzuki K, Soga N, Hanada T. 1995. Mechanisms and concentration dependence of Tm^{3+} blue and Er^{3+} green up-conversion in codoped glasses by red-laser pumping. *J. Lumin.* 65:247–55
25. Feist JP, Heyes AL, Seefeldt S. 2003. Oxygen quenching of phosphorescence from thermographic phosphors. *Meas. Sci. Tech.* 14:N17–20
26. Maloney MJ. 2001. *U.S. Patent No. 6,284,323*
27. Maloney MJ. 2000. *U.S. Patent No. 6,117,560*
28. Wu J, Wei XZ, Padture NP, Klemens PG, Gell M, et al. 2002. Low-thermal-conductivity rare-earth zirconates for potential thermal-barrier-coating applications. *J. Am. Ceram. Soc.* 85:3031–35
29. Kraemer S, Yang J, Levi CG. 2008. Infiltration-inhibiting reaction of gadolinium zirconate thermal barrier coatings with CMAS melts. *J. Am. Ceram. Soc.* 91:576–83
30. Kraemer S, Yang J, Levi CG, Johnson CA. 2006. Thermochemical interaction of thermal barrier coatings with molten CaO-MgO-Al_2O_3-SiO_2 (CMAS) deposits. *J. Am. Ceram. Soc.* 89:3167–75
31. Chambers MD, Clarke DR. 2007. Terbium as an alternative for luminescence sensing of temperature of thermal barrier coating materials. *Surf. Coat. Technol.* 202:688–92
32. Lin H, Yang DL, Liu GS, Ma TC, Zhai B, et al. 2005. Optical absorption and photoluminescence in Sm^{3+}- and Eu^{3+}-doped rare-earth borate glasses. *J. Lumin.* 113:121–28
33. Gentleman MM. 2006. *High temperature sensing of thermal barrier materials by luminescence*. PhD thesis. Univ. Calif., Santa Barbara
34. Lee KN, Fox DS, Bansal NP. 2005. Rare earth silicate environmental barrier coatings for SiC/SiC composites and Si_3N_4 ceramics. *J. Eur. Ceram. Soc.* 25:1705–15
35. Belmonte M. 2006. Advanced ceramic materials for high temperature applications. *Adv. Eng. Mater.* 8:693–703
36. Shannon RD, Prewitt CT. 1969. Effective ionic radii in oxides and fluorides. *Acta Crystallogr.* B25:925–46
37. Shannon RD. 1976. Revised effective ionic radii and systematic studies of interatomic distances in halides and chalcogenides. *Acta Crystallogr.* A32:751–67
38. Liu Y, Xu CN, Chen H, Tateyama H. 2002. Influence of calcining temperature on photoluminescence and thermal quenching in europium-doped Y_2SiO_5 using the MOD process. *J. Lumin.* 97:135–40
39. Cannas C, Mainas M, Musinu A, Piccaluga G, Enzo S, et al. 2007. Structural investigations and luminescence properties of nanocrystalline europium-doped yttrium silicates prepared by a sol–gel technique. *Opt. Mater.* 29:585–92
40. Leonyuk NI, Belokoneva EL, Bocelli G, Righi L, Shvanskii EV, et al. 1999. Crystal growth and structural refinements of the Y_2SiO_5, $Y_2Si_2O_7$ and $LaBSiO_5$ single crystals. *Cryst. Res. Technol.* 34:1175–82

41. Zhang QY, Pita K, Buddhuhu S, Kam CH. 2002. Luminescent properties of rare-earth ion doped yttrium silicate thin film phosphors for a full-colour display. *J. Phys. D* 35:3085–90
42. Christensen AN, Hazell RG, Hewat AW. 1997. Synthesis, crystal growth and structure investigations of rare-earth disilicates and rare-earth oxyapatites. *Acta Chem. Scand.* 51:37–43
43. Felsche J. 1970. Polymorphism and crystal data of the rare-earth disilicates of the type $R.E._2Si_2O_7$. *J. Less Common Met.* 21:1–14
44. Aparicio M, Duran A. 2000. Yttrium silicate coatings for oxidation protection of carbon-silicon carbide composites. *J. Am. Ceram. Soc.* 83:1351–55
45. Seifert HJ, Wagner S, Fabrichnaya O, Lukas HL, Aldinger F, et al. 2005. Yttrium silicate coatings on chemical vapor deposition-SiC-precoated C/C-SiC: thermodynamic assessment and high-temperature investigation. *J. Am. Ceram. Soc.* 88:424–30
46. Kremenovic A, Colomban PH, Piriou B, Massiot D, Florian P. 2003. Structural and spectroscopic characterization of the quenched hexacelsian. *J. Phys. Chem. Solids* 64:2253–68
47. Blasse G. 1975. Influence of local charge compensation on site occupation and luminescence of apatites. *J. Solid State Chem.* 14:181–84
48. Duignan JP, Oswald IDH, Sage IC, Sweeting LM, Tanaka K, et al. 2002. Do triboluminescent spectra really show a spectral shift relative to photoluminescence spectra? *J. Lumin.* 97:115–26
49. Ishihara T, Tanaka K, Fujita K, Hirao K, Soga N. 1998. Full color triboluminescence of rare-earth-doped hexacelsian ($BaAl_2Si_2O_8$). *Solid State Commun.* 107:763–67
50. Ishihara T, Tanaka K, Hirao K, Soga N. 1997. Fracto-luminescence of rare earth element-doped hexacelsian ($BaAl_2Si_2O_8$). *Jpn. J. Appl. Phys.* 36:L781–83
51. Lee KN, Fox DS, Eldridge JI, Zhu DM, Robinson RC, et al. 2003. Upper temperature limit of environmental barrier coatings based on mullite and BSAS. *J. Am. Ceram. Soc.* 86:1299–306
52. Chambers MD, Rousseve PA, Clarke DR. 2008. Decay pathway and high temperature luminescence of Eu^{3+} in $Ca_2Gd_8Si_6O_{26}$. *J. Lumin.* 129:263–69
53. Yu M, Lin J, Zhou YH, Wang SB, Zhang HJ. 2002. Sol-gel deposition and luminescent properties of oxyapatite $Ca_2(Y,Gd)_8(SiO_4)_6O_2$ phosphor films doped with rare earth and lead ions. *J. Mater. Chem.* 12:86–91
54. Kaminskii AA. 1990. *Laser Crystals*. Berlin: Springer-Verlag
55. Hess NJ, Schiferl D. 1990. Pressure and temperature dependence of laser-induced fluorescence of Sm:YAG to 100 kbar and 700°C and an empirical model. *J. Appl. Phys.* 68:1953–60
56. Dorenbos P. 2000. The $4f^n \leftrightarrow 4f^{n-1}5d$ transitions of the trivalent lanthanides in halogenides and chalcogenides. *J. Lumin.* 91:91–106
57. Dorenbos P. 2003. Systematic behaviour in trivalent lanthanide charge transfer energies. *J. Phys. Condens. Matter* 15:8417–34
58. Gulgun MA, Voytovych R, Maclaren I, Rühle M, Cannon RM. 2002. Cation segregation in an oxide ceramic with low solubility: yttrium doped alpha-alumina. *Interface Science* 10:99–110
59. Cawley JD, Halloran JW. 1986. Dopant distribution in nominally yttrium-doped sapphire. *J. Am. Ceram. Soc.* 69:C195–96
60. Thompson AM, Soni KK, Chan HM, Harmer MP, Williams DB, et al. 1997. Dopant distributions in rare-earth-doped alumina. *J. Am. Ceram. Soc.* 80:373–76
61. Seat HC, Sharp JH. 2004. Dedicated temperature sensing with *C*-axis oriented single-crystal ruby (Cr^{3+}:Al_2O_3) fibers: temperature and strain dependences of *R*-line fluorescence. *IEEE Trans. Instrum. Meas.* 53:140–54
62. Seat HC, Sharp JH, Zhang ZY, Grattan KTV. 2002. Single-crystal ruby fiber temperature sensor. *Sens. Actuators A* 101:24–29
63. Hu YL, Zhang ZY, Gratten KTV, Palmer AW, Meggitt BT. 1997. Ruby-based decay-time thermometry: effect of probe size on extended measurement range (77–800 K). *Sens. Actuators A* 63:85–90
64. Pflitsch C, Siddiqui RA, Atakan B. 2008. Phosphorescence properties of sol-gel derived ruby measured as functions of temperature and Cr^{3+} content. *Appl. Phys. A* 90:527–32
65. Duclos SJ, Vohra YK, Ruoff AL. 1990. Pressure dependence of the $^4T_2$ and $^4T_1$ absorption bands of ruby to 35 GPA. *Phys. Rev. B* 41:5372–81

66. Margueron SH, Clarke DR. 2007. Stress anisotropy of *R*-line luminescence lifetime in single crystal Cr-doped sapphire (ruby). *J. Appl. Phys.* 101:93521
67. Margueron SH, Clarke DR. 2007. Effect of residual stress on the luminescence lifetime of *R*-line emission from polycrystalline alumina formed by oxidation. *J. Am. Ceram. Soc.* 90:1798–801
68. Lyo SK. 1971. Critical concentration for single-ion-single-ion energy transfer in ruby. *Phys. Rev. B* 3:3331–41
69. Marshall CD, Payne PA, Smith LK, Powell HT, Krupke WF, Chai BHT. 1995. 1.047-μm $Yb:Sr_5(PO_4)_3F$ energy storage optical amplifier. *IEEE J. Sel. Top. Quant. Elect.* 1:67–77
70. Dwivedi RK, Kay DAR. 1984. Determination of the standard free energies of formation of Ce_2O_2S and Y_2O_2 at high temperatures. *J. Less Common Met.* 102:1–7
71. Tsai MS, Hon MH. 1994. Phase formation and thermal stability of calcium lanthanum sulfide powder. *Ceram. Int.* 20:303–8
72. McCallum JC, Morpeth LD. 1999. Synthesis of Ti:sapphire by ion implantation. *Nucl. Instrum. Meth. Phys. Res. B* 148:726–29
73. Eldridge JI, Bencic TJ. 2006. Monitoring delamination of plasma-sprayed thermal barrier coatings by reflectance-enhanced luminescence. *Surf. Coat. Technol.* 201:3926–30
74. Eldridge JI, Singh J, Wolfe DE. 2006. Erosion-indicating thermal barrier coatings using luminescent sublayers. *J. Am. Ceram. Soc.* 89:3252–54
75. Eldridge JI, Bencic TJ, Allison SW, Beshears DL. 2004. Depth-penetrating temperature measurements of thermal barrier coatings incorporating thermographic phosphors. *J. Therm. Spray Technol.* 13:44–50
76. Chen X, Mutasim Z, Price J, Feist JP, Heyes AL, Seefeldt AL. 2005. Industrial sensor TBCs: studies on temperature detection and durability. *Int. J. Appl. Ceram. Technol.* 2:414–21
77. Ramos-Brito F, Garcia-Hipolito M, Alejo-Armenta C, Alvarez-Fragoso O, Falcony C. 2007. Characterization of luminescent praseodymium-doped ZrO_2 coatings deposited by ultrasonic spray pyrolysis technique. *J. Phys. D* 40:6718–24
78. Feist JP, Heyes AL, Seefeldt S. 2003. Thermographic phosphor thermometry for film cooling studies in gas turbine combustions. *Proc. Inst. Mech. Eng.* 217:193–200
79. Chambers MD, Clarke DR. 2006. Effect of long-term, high temperature aging on luminescence from Eu-doped YSZ thermal barrier coatings. *Surf. Coat. Technol.* 201:3942–46
80. Gentleman MM, Eldridge JI, Zhu DM, Murphy KS, Clarke DR. 2006. Non-contact sensing of TBC/BC interface temperature in a thermal gradient. *Surf. Coat. Technol.* 201:3937–41
81. Muratori C, Clarke DR, Jones JG, Voevodin AA. 2008. Smart tribological coatings with wear sensing capability. *Wear* 265:913–20
82. Kilo M, Taylor MA, Argirusis C, Borchardt G, Lesage B, et al. 2003. Cation self-diffusion of ^{44}Ca, ^{88}Y, and ^{96}Zr in single-crystalline calcia- and yttria-doped zirconia. *J. Appl. Phys.* 94:7547–52
83. Leckie RM, Kramer S, Rühle M, Levi CG. 2005. Thermochemical compatibility between alumina and ZrO_2-$GdO_{3/2}$ thermal barrier coatings. *Acta Mater.* 53:3281–92
84. Morgan PED, Marshall DB. 1995. Ceramic composites of monazite and alumina. *J. Am. Ceram. Soc.* 78:1553–63
85. Winter MR, Clarke DR. 2007. Oxide materials with low thermal conductivity. *J. Am. Ceram. Soc.* 90:533–40
86. Miller MP, Wright JC. 1979. Multiphonon and energy transfer relaxation in charge compensated crystals. *J. Chem. Phys.* 71:324–38
87. Riseberg LA, Moos HW. 1968. Multiphonon orbit-lattice relaxation of excited states of rare-earth ions in crystals. *Phys. Rev.* 174:429–38
88. Fonger WH, Struck CW. 1969. Eu^{3+} ^5D resonance quenching to charge-transfer states in Y_2O_2S, La_2O_2S, and LaOCl. *J. Chem. Phys.* 52:6364–72
89. Struck CW, Fonger WH. 1975. Quantum-mechanical treatment of Eu^{3+} $4f \rightarrow 4f$ and $4f$-charge-transfer-state transitions in Y_2O_2S and La_2O_2S. *J. Chem. Phys.* 64:1784–90
90. Englman R, Jortner J. 1970. Energy gap law for radiationless transitions in large molecules. *Mol. Phys.* 18:145–64

91. Cavalli E, Bovero E, Magnani N, Ramirez MO, Speghini A, Bettinelli M. 2003. Optical spectroscopy and crystal-field analysis of $YAl_3(BO_3)_4$ single crystals doped with dysprosium. *J. Phys. Condens. Matter* 15:1047–56
92. Dexter DL, Schulman JH. 1954. Theory of concentration quenching in inorganic phosphors. *J. Chem. Phys.* 22:1063–70
93. Varsanyi F, Dieke GH. 1961. Ion-pair resonance mechanism of energy transfer in rare earth crystal fluorescence. *Phys. Rev. Lett.* 7:442–44
94. Weber MJ. 1971. Luminescence decay by energy migration and transfer: observation of diffusion-limited relaxation. *Phys. Rev. B* 4:2932–39
95. Gruber JB, Nash KL, Yow RM, Sardar DK, Valiev UV, et al. 2008. Spectroscopic and magnetic susceptibility analysis of the ^7F_J and $^5D_4$ energy levels of Tb^{3+} ($4f^8$) in $TbAlO_3$. *J. Lumin.* 128:1271–84
96. Van Uitert LG, Iida S. 1962. Quenching interactions between rare-earth ions. *J. Chem. Phys.* 37:986–92
97. Van Uitert LG, Johnson LF. 1966. Energy transfer between rare-earth ions. *J. Chem. Phys.* 44:3514–22
98. Allison SW, Goedeke SM, Cates MR, Hollerman HA, Eldridge JI, Bencic TJ. 2005. Fluorescence rise time measurements for high temperature fluorescence-based thermometry. *Oak Ridge Natl. Lab. Rep. R05-123055*
99. Ranson RM, Evangelou E, Thomas CB. 1998. Modeling the fluorescent lifetime of Y_2O_3:Eu. *Appl. Phys. Lett.* 72:2663–64
100. Zhang ZY, Grattan KTV, Palmer AW. 1991. A novel signal processing scheme for a fluorescence based fiber-optic temperature sensor. *Rev. Sci. Instrum.* 62:1735–42
101. Rosso L, Fernicola VC. 2006. Time- and frequency-domain analyses of fluorescence lifetime for temperature sensing. *Rev. Sci. Instrum.* 77:034901
102. Grinberg M, Holliday K. 2001. Luminescence kinetics and emission lifetime distribution of Cr^{3+}-doped aluminosilicate glass. *J. Lumin.* 92:277–86
103. Walker DG, Allison SW. 2007. Transient measurements using thermographic phosphors. *ISA Trans.* 46:15–20
104. O'Connor DV, Phillips D. 1985. *Time-Correlated Single-Photon Counting*. London: Academic
105. Seyfried H, Richter M, Alden M, Schmidt H. 2007. Laser-induced phosphorescence for surface thermometry in the afterburner of an aircraft engine. *AIAA J.* 45:2966–71
106. Mannik L, Brown SK, Campbell SR. 1987. Phosphor-based thermometry of rotating surfaces. *Appl. Opt.* 26:4014–17
107. Tobin KW, Allison SW, Cates MR, Capps GJ, Beshears DL, et al. 1990. High-temperature phosphor thermometry of rotating turbine blades. *AIAA J.* 28:1485–90
108. Sasaki K, Masuhara H. 1991. Analysis of transient emission curves by a convolved autoregressive model. *Appl. Opt.* 30:977–80
109. Enderlein J, Erdmann R. 1997. Fast fitting of multi-exponential decay curves. *Opt. Commun.* 134:371–78
110. Novikov EG. 1998. Error estimation in the phase plane method of multi-exponential decay analysis. *Opt. Commun.* 151:313–20
111. Zhang ZY, Grattan KTV, Hui YL, Palmer AW, Meggitt BT. 1996. Prony's method for exponential lifetime estimations in fluorescence-based thermometers. *Rev. Sci. Instrum.* 67:2590–94
112. Reisfeld R, Greenberg E, Velapoldi R. 1972. Luminescence quantum efficiency of Gd and Tb in borate glasses and the mechanism of energy transfer between them. *J. Chem. Phys.* 56:1698–705
113. Naccache R, Vetrone F, Speghini A, Bettinelli M, Capobianco JA. 2008. Cross-relaxation and upconversion processes in Pr^{3+} singly doped and Pr^{3+}/Yb^{3+} codoped nanocrystalline $Gd_3Ga_5O_{12}$: the sensitizer/activator relationship. *J. Phys. Chem. C* 112:7750–56
114. Walker DG. 2005. Heat flux determination from measured heating rates using thermographic phosphors. *Trans. ASME* 127:560–70
115. Omrane A, Ossler F, Alden M, Svenson J, Pettersson JBC. 2005. Surface temperature of decomposing construction materials studied by laser-induced phosphorescence. *Fire Mater.* 29:39–51
116. Brubach J, Patt A, Dreizler A. 2006. Spray thermometry using thermographic phosphors. *Appl. Phys. B* 83:499–502
117. Allison SW, Cates MR, Goedeke SM, Akerman A, Crawford M, et al. 2007. In-flight armature diagnostics. *IEEE Trans. Magn.* 43:329–33

118. Judd BR. 1962. Optical absorption intensities of rare-earth ions. *Phys. Rev.* 127:750–61
119. Ofelt GS. 1962. Intensities of crystal spectra of rare-earth ions. *J. Chem. Phys.* 37:511–20
120. Dieke GH. 1968. *Spectra and Energy Levels of Rare Earth Ions in Crystals*, ed. HM Crosswhite, H Crosswhite. New York: Interscience
121. Carnall WT, Fields PR, Rajnak K. 1968. Electronic energy levels in the trivalent lanthanide aquo ions. I. Pr^{3+}, Nd^{3+}, Pm^{3+}, Sm^{3+}, Dy^{3+}, Ho^{3+}, Er^{3+}, and Tm^{3+}. *J. Chem. Phys.* 49:4424–42
122. Carnall WT, Fields PR, Rajnak K. 1968. Spectral intensities of the trivalent lanthanides and actinides in solution. II. Pm^{3+}, Sm^{3+}, Eu^{3+}, Gd^{3+}, Tb^{3+}, Dy^{3+}, and Ho^{3+}. *J. Chem. Phys.* 49:4412–23
123. Shen Y, Clarke DR. 2008. Effects of reducing atmosphere on the luminescence of $Eu3^{+}$-doped yttria-stabilized zirconia sensor layers in thermal barrier coatings. *J. Am. Ceram. Soc.* 92:125–29
124. Alaruri SD, Brewington AJ, Thomas MA, Miller JA. 1993. High-temperature remote thermometry using laser-induced fluorescence decay lifetime measurements of Y_2O_3:Eu and YAG:Tb thermographic phosphors. *IEEE Trans. Instrum. Meas.* 42:735–39
125. Zhang ZY, Grattan KTV, Palmer AW, Meggitt BT. 1997. Potential for temperature sensor applications of highly neodymium-doped crystals and fiber at up to approximately 1000°C. *Rev. Sci. Instrum.* 68:2759–63
126. Cates MR, Allison SW, Jaiswal SL, Beshears DL. 2003. *YAG:Dy and YAG:Tm fluorescence to 1700°C.* Presented at ISA Int. Instrum. Symp., 49th, Orlando
127. Collins SF, Baxter GW, Wade SA, Sun T, Gratten KTV, et al. 1998. Comparison of fluorescence-based temperature sensor schemes: theoretical analysis and experimental validation. *J. Appl. Phys.* 84:4649–54
128. Hollerman WA, Allison SW, Goedeke SM, Boudreaux P, Guidry R, Gates E. 2003. Comparison of fluorescence properties for single crystal and polycrystalline YAG:Ce. *IEEE Trans. Nucl. Sci.* 50:754–57
129. Allison SW, Gillies GT, Rondinone AJ, Cates MR. 2003. Nanoscale thermometry via the fluorescence of YAG:Ce phosphor particles: measurements from 7 to 77°C. *Nanotechnology* 14:859–63
130. Djeu N, Kennedy JL, Djeu D. 2007. Thermally compensated temperature sensor capable of highly accurate measurements on surfaces. *Rev. Sci. Instrum.* 78:094901
131. Zhang ZY, Grattan KTV, Meggitt BT. 2000. Thulium-doped fiber optic decay-time temperature sensors: characterization of high temperature performance. *Rev. Sci. Instrum.* 71:1614–20
132. Allison SW, Beshears DL, Bencic T, Hollerman WA, Boudreaux P. 2001. Development of temperature-sensitive paints for high temperature aeropropulsion applications. *Proc. Jt. Propuls. Conf. AIAA, 37th, Salt Lake City*, AIAA-2001-3528
133. Allison SW, Beshears DL, Gadfort T, Bencic T, Eldridge J, et al. 2001. High temperature surface measurements using lifetime imaging of thermographic phosphors: bonding tests. *Proc. Int. Congr. Instrum. Aerosp. Simul. Facil., 19th*
134. Zhang ZY, Grattan KTV, Palmer AW. 1992. Fiber-optic high-temperature sensor based on the fluorescence lifetime of alexandrite. *Rev. Sci. Instrum.* 63:3869–73
135. Sliney JG, Leung KM, Birnbaum M, Tucker AW. 1979. Lifetimes of the $^4F_{3/2}$ state in Nd:YVO_4. *J. Appl. Phys.* 50:3778–79
136. Allison SW, Goedeke SM, Beshears DL, Cates MR, Hollerman WA, et al. 2003. Advances in high temperature phosphor thermometry for aerospace applications. *AIAA/ASME/SAE/ASEE Jt. Propuls. Conf., 39th, Huntsville, AL*, 73:1832–34
137. Alaruri SD, McFarland D, Brewington AJ, Thomas MA, Sallee N. 1995. Development of a fiber-optic probe for thermographic phosphor measurements in turbine engines. *Opt. Lasers Eng.* 22:17–31
138. Ranson RM, Thomas CB, Craven MR. 1998. A thin film coating for phosphor thermography. *Meas. Sci. Technol.* 9:1947–50
139. Zhydachevskii Y, Galanciak D, Kobyakov S, Berkowski M, Kaminska A, et al. 2006. Photoluminescence studies of Mn^{4+} ions in $YAlO_3$ crystals at ambient and high pressure. *J. Phys. Condens. Matter* 18:11385–96
140. Bugos AR, Allison SW, Cates MR. 1989. Emission properties of europium-doped lanthanum and lutetium orthosphosphate crystals for use in high temperature sensor applications. *IEEE Proc. Southeast Conf., Columbia, SC*, 1:361–65
141. Bugos AR, Allison SW, Cates MR. 1991. Laser-induced fluorescent properties of europium-doped scandium orthophosphate phosphors for high-temperature sensing applications. *IEEE Proc. Southeast Conf., Williamsburg, VA* 1&2:1143–47

142. Lozykowski HJ, Jadwisienczak WM. 2007. Thermal quenching of luminescence and isovalent trap model for rare-earth-ion-doped AlN. *Phys. Status Solidi* 244:2109–26
143. Shen YR, Bray KL. 1998. Effect of pressure and temperature on 4*f*-4*f* luminescence properties of Sm^{2+} ions in *M*FCl crystals (*M* = Ba, Sr, and Ca). *Phys. Rev. B* 58:11944–58
144. Feist JP, Heyes AL. 2000. The characterization of Y_2O_2S:Sm powder as a thermographic phosphor for high temperature applications. *Meas. Sci. Technol.* 11:942–47
145. Allison SW, Cates MR, Goedeke SM. 2005. Thermometry for single events and fast response. *Proc. Int. Instrum. Symp.* 457:81–90
146. McSherry M, Lewis E, Fitzpatrick C. 2005. Development of temperature sensitive glassware for monitoring temperatures in harsh industrial environments. *Sensors Actuators* 123–124:408–17
147. Sun T, Zhang ZY, Grattan KTV, Palmer AW, Collins FW. 1997. Temperature dependence of the fluorescence lifetime in Pr^{3+}:ZBLAN glass for fiber optic thermometry. *Rev. Sci. Instrum.* 68:3447–45
148. Sokolska I, Golab S, Baluka M, Ryba-Romanowski W. 2000. Quenching of Pr^{3+} emission in single crystals of $K_5Pr_xLa_{1-x}Li_2F_{10}$. *J. Lumin.* 91:79–86
149. Mitchell IR, Farrell PM, Baxter GW, Collins SF, Grattan KTV, Sun T. 2000. Analysis of dopant concentration effects in praseodymium-based fluorescent fiber optic temperature sensors. *Rev. Sci. Instrum.* 71:100–3
150. Gusowski MA, Doniniak-Dzik G, Solarz P, Lisiecki R, Ryba-Romanowski W. 2007. Luminescence and energy transfer in K_3GdF_6:Pr^{3+}. *J. Alloys Compd.* 438:72–76
151. Vetter U, Gruber JB, Nijjar AS, Zandi B, Öhl G, et al. 2006. Crystal field analysis of Pm^{3+} ($4f^4$) and Sm^{3+} ($4f^5$) and lattice location studies of ^{147}Nd and ^{147}Pm in *w*-AlN. *Phys. Rev. B* 74:205201
152. Luxbacher T, Fritzer HP, Flint CD. 1997. Temperature dependence of luminescence decay from the $^4G_{5/2}$ state of Sm^{3+} in $Cs_2NaSm_xY_{1-x}Cl_6$ and $Cs_2NaSm_xEu_yY_{1-x-y}Cl_6$. *J. Lumin.* 71:313–19
153. Lin J, Su Q. 1995. Luminescence and energy transfer of rare-earth-metal ions in $Mg_2Y_8(SiO_4)_6O_2$. *J. Mater. Chem.* 5:1151–54
154. Liu LQ, Chen XY. 2007. Energy levels, fluorescence lifetime and Judd-Ofelt parameters of Eu^{3+} in Gd_2O_3 nanocrystals. *Nanotechnology* 18:255704
155. Kobayasi T, Mroczkowski S, Owen JF. 1980. Fluorescence lifetime and quantum efficiency for 5d→4f transitions in Eu^{2+} doped chloride and fluoride crystals. *J. Lumin.* 21:247–57
156. Poort SHM, Meyerink A, Blasse G. 1997. Lifetime measurements in Eu^{2+}-doped host lattices. *J. Phys. Chem. Solids* 58:1451–56
157. Kellendonk F, Blasse G. 1981. On the luminescence of Sm^{3+}, Gd^{3+}, and Dy^{3+} in yttrium aluminum borate. *Phys. Stat. Sol. B* 108:541–48
158. Xu LW, Crosswhite HM, Hessler JP. 1984. Fluorescent and dynamic properties of optically excited dysprosium trifluoride. *J. Chem. Phys.* 81:698–703
159. Lal B, Rao DR. 1978. Fluorescence and lifetime studies of Ho^{3+}:CaF_2. *Chem. Phys. Lett.* 53:250–54
160. Lorenzo A, Bausa LE, Sanz Garcia JA, Garcia Sole J. 1996. Optical absorption intensities and fluorescence dynamics of Ho^{3+} ions in $LiNbO_3$. *J. Phys. Condens. Matter* 8:5781–91
161. Wang WM, Yin YS, Yuan DR. 2007. Optical transitions in Ho^{3+} doped $La_3Gd_5SiO_{14}$ crystals. *J. Alloys Compd.* 436:364–68
162. Zhang ZY, Grattan KTV, Palmer AW, Meggitt BT, Sun T. 1998. Characterization of erbium-doped intrinsic optical fiber sensor probes at high temperatures. *Rev. Sci. Instrum.* 69:2924
163. Sun T, Zhang ZY, Grattan KTV. 2000. Erbium-ytterbium fluorescence based fiber optic temperature sensor system. *Rev. Sci. Instrum.* 71:4017–22
164. Zhang HW, Fu XY, Niu SY, Xin Q. 2008. Blue luminescence of nanocrystalline $CaZrO_3$:Tm phosphors synthesized by a modified Pechini sol-gel method. *J. Lumin.* 128:1348–52
165. Sun T, Zhang ZY, Grattan KTV, Palmer AW. 1998. Ytterbium-based fluorescence decay time fiber optic temperature sensor systems. *Rev. Sci. Instrum.* 69:4179–85
166. Yang PZ, Deng PZ, Yin ZW. 2002. Concentration quenching in Yb:YAG. *J. Lumin.* 97:51–54

Annual Review of
Materials Research

Volume 39, 2009

Contents

Materials Advances for Next-Generation Microelectronics

Current Interest

Index

Errata

An online log of corrections to *Annual Review of Materials Research* articles may be found at http://matsci.annualreviews.org/errata.shtml